



Degree Project in Technology

First cycle, 15 credits

# **Electric propulsion of satellites as an alternative for implementation of a sunshade system**

**MAHEEN ARFAN, ISABELLE BONNIER**



# Electric propulsion of satellites as an alternative for implementation of a sunshade system

Maheen Arfan and Isabelle Bonnier  
SA114X Degree Project in Engineering Physics, First Level

Royal Institute of Technology (KTH)

June 1, 2022

## Abstract

As an alternative solution to global warming, this thesis explores the possibility of a space-based geoengineering scheme that may prove worthwhile to implement in parallel to other environmental efforts that help mitigate impact of climate change. One suggestion of a geoengineering solution is deploying a large number of sunshades in the vicinity of the first Lagrange point of the Sun-Earth system, and this prospective sunshade project would serve to shield Earth from incident solar radiation. This thesis is an extension of a feasibility study for the implementation of this large-scale mission, and has a focus on comparing electric thrusters to solar sailing as a means of propulsion. Background on electric propulsion systems and spaceflight mechanics is provided. The investigation was performed by defining the spacecraft configurations, and then computing trajectories to a point of escape from Earth and from there to the final equilibrium point.

Our results show that in order to meet the propellant demands of the electric thrusters, the launch mass would need to increase by around 15-25 % compared to the solar sailing implementation, equating to around  $10^{10}$  kg. Nevertheless, electric propulsion could still be a beneficial choice since it would allow shorter transfer times for each shade which reduces the radiation exposure and subsequent degradation of the spacecraft's systems. It was found that the transfer time with electric propulsion would be about one-half or one-fifth that of solar sailing, depending on spacecraft parameters. Additionally, electric propulsion allows a much lower initial parking orbit, and while this would increase the radiation exposure it would also reduce the launch costs due to the higher payload capacity to lower altitudes. However, electric propulsion of this scale require prior advancements in xenon or other inert propellant extraction methods and possibly a wide-scale construction of air separation plants.

## Sammanfattning

Som en alternativ lösning på global uppvärmning undersöker denna uppsats möjligheten till ett rymdbaserat geoengineering-system som kan visa sig vara värt att implementera parallellt med andra miljöinsatser som hjälper till att mildra effekterna av klimatförändringar. Ett förslag på en geoteknisk lösning är att placera ut ett stort antal solparasoll i närheten av den första Lagrange-punkten i sol-jord systemet, och detta blivande solparasollsystem skulle syfta till att skydda jorden från infallande solstrålning. Detta examensarbete är en förlängning av en studie om genomförbarheten av detta storskaliga uppdrag, och har ett fokus på att jämföra elektriska thrusters med solsegling som framdrivningsmedel. Bakgrund om elektriska framdrivningssystem och rymdfärdsmechanik tillhandahålls. Undersökningen utfördes genom att definiera rymdskeppsconfigurationerna och sedan beräkna banor för en flykt från jorden och därifrån till den slutliga jämviktspunkten.

Våra resultat visar att för att möta kraven på drivmedel hos de elektriska motorerna, skulle launch-massan behöva öka med cirka 15-25 % jämfört med solsegling-implementationen, vilket motsvarar cirka  $10^{10}$  kg. Ändå kan elektrisk framdrivning fortfarande vara ett fördelaktigt val eftersom det skulle tillåta kortare transporttider för varje parasoll, vilket minskar strålningsexponeringen och efterföljande degradering av rymdfarkostens system. Det visades att transporttiden med elektrisk framdrivning skulle vara ungefär hälften eller en femtedel av den för solsegling, beroende på rymdfarkostparametrar. Dessutom tillåter elektrisk framdrivning en mycket lägre initial parkeringsbana, och även om detta skulle öka strålningsexponeringen skulle det också minska launch-kostnaderna på grund av den högre nyttolastkapaciteten till lägre höjder. Elektrisk framdrivning av denna skala kräver emellertid föregående utveckling av metoder för utvinning av xenon eller andra inerta drivmedel och eventuellt en storskalig konstruktion av luftseparationsanläggningar.

## Acknowledgements

We would like to thank our supervisor Christer Fuglesang for his continuous help and feedback with this project, as well as María García de Herreros Miciano for answering additional questions. We would also like to extend thanks to Benjamin Jouanneau for the invaluable help with the numerical implementation.

# Contents

<b>1</b>	<b>Introduction</b>	<b>4</b>
<b>2</b>	<b>Background Material</b>	<b>6</b>
2.1	Sunshade project . . . . .	6
2.1.1	What is the sunshade project? . . . . .	6
2.1.2	Choice of propulsion system . . . . .	6
2.1.3	Solar sailing in numbers . . . . .	7
2.2	Electric propulsion . . . . .	8
2.2.1	Ideal rocket equation . . . . .	8
2.2.2	Types of electric propulsion thrusters and how they work . . . . .	9
2.2.3	Parameters of electric propulsion thrusters . . . . .	10
2.2.4	Power sources and solar cells . . . . .	10
2.2.5	Propellants . . . . .	11
2.2.6	Current electric propulsion thrusters . . . . .	12
2.3	Orbital mechanics . . . . .	12
2.3.1	Two-body problem . . . . .	12
2.3.2	Low-thrust orbit transfer and delta-V budget . . . . .	14
2.3.3	The restricted three body problem . . . . .	15
2.3.4	Sun-Earth Lagrange points . . . . .	17
2.3.5	Solar pressure and sub-Lagrange point . . . . .	17
<b>3</b>	<b>Investigation</b>	<b>19</b>
3.1	Problem . . . . .	19
3.1.1	Optimal control problem . . . . .	19
3.2	Model . . . . .	20
3.2.1	Two body problem equations in polar coordinates . . . . .	20
3.2.2	Characteristic Quantities and Nondimensionalisation in the Circular Restricted Three-Body Problem . . . . .	21
3.2.3	Coordinate systems . . . . .	22
3.2.4	Optimal control problem in three-body dynamics . . . . .	25
3.3	Analytical Calculations . . . . .	25
3.3.1	Delta-V budget for ion propulsion . . . . .	25
3.4	Numerical Analysis . . . . .	27
3.4.1	Two-body problem . . . . .	27
3.4.2	Three-body problem . . . . .	28
3.5	Results . . . . .	28
3.5.1	Choice of ion thruster . . . . .	28

3.5.2	Escape time for different initial parking orbits . . . . .	30
3.5.3	Escape trajectory for sunshade system . . . . .	31
3.5.4	Travel to the sub-Lagrange point . . . . .	32
<b>4</b>	<b>Discussion and Conclusions</b>	<b>37</b>
4.1	Discussion . . . . .	37
4.1.1	Partial and full trajectory with ion propulsion . . . . .	37
4.1.2	Initial parking orbits and number of launches . . . . .	38
4.1.3	Chemical propulsion to geostationary orbit . . . . .	38
4.1.4	Environmental impact and production . . . . .	39
4.1.5	Solar sail area and feasibility . . . . .	40
4.1.6	Accuracy and assumptions . . . . .	40
4.2	Summary and Conclusions . . . . .	42

# Chapter 1

## Introduction

One of the greatest challenges facing our society today is global warming. The greenhouse effect, magnified by emissions of gases that trap heat in the Earth's atmosphere, has caused the global mean temperature to rise by 1 °C since pre-industrial times [1]. Consequences of increasing temperatures is a subject currently undergoing rigorous study but have already proven disastrous for both the environment and society, as links have been found to extreme weather and droughts, loss of biodiversity, and rising sea levels [2]. As a unifying measure and to prevent further climate changes, the Paris Agreement was signed in 2015 by 196 parties. The agreement sets forth goals to limit the global warming to 1.5 - 2 °C, and in the wake of this many countries and companies have started instituting their own carbon neutrality goals and inventing zero-carbon solutions in order to reach them [3].

Even so, due to the rapidly advancing rate of temperature increase it is possible that these measures are not enough to ward off non-reversible changes to our planet. Instead, alternative solutions are being investigated, ones that are not merely preventative and can be implemented in parallel. Other than just focusing on reducing the emissions of greenhouse gases, more direct action can be taken in the form of capture and removal of already emitted carbon dioxide from the atmosphere (carbon sequestration) or artificial shielding from the amount of solar radiation that either reaches or is retained by the Earth's atmosphere [4]. These are examples of geoengineering, a currently mainly conceptual idea of large-scale alterations performed on a planet's climate system. Space-based geoengineering, such as the deployment of shades outside of the Earth's atmosphere with the aim of reducing the amount of incident solar radiation, has also been put forward as a less invasive and more easily reversible option.

A feasibility study of the implementation of such a shade system was performed in [5] and [6]. The study focused on how a shade system could be put into place in practice, as well as providing estimations of the cost and the impact of such a project. In part, the use of solar sailing as a means of propulsion for transporting the shades was investigated, as there are many similarities between a proposed sunshade and solar sails. While the execution of a sunshade system is still far off, the novelty of solar sailing might hinder its progression. A more mature form of propulsion is electric propulsion, which has to date been used in many successful spaceflight missions and is well suited for interplanetary transfers.

This study will therefore focus on this type of propulsion as an alternative to solar sailing, and compare the results with those found in the original thesis. First, the literature study will provide the necessary information on electric propulsion, its types and features, in order to make estimations of the composition of the spacecrafts. The section regarding orbital mechanics details the equations which would govern the dynamics of a satellite's trajectory as it transfers from Earth to the final position. Thereafter analytical and numerical calculations determine what amount of mass and time the sunshade project would require, and this is equated to costs and compared to the results from when solar sailing was used.

# Chapter 2

## Background Material

### 2.1 Sunshade project

The implementation of a large-scale sunshade outside of Earth is a project spanning many years, and this section details the history of the project, the focus of this thesis, as well as the results which have already been obtained by previous studies and which will be used for comparisons.

#### 2.1.1 What is the sunshade project?

The idea of reducing the amount of solar radiation received by Earth via a physical shield was put forward in 1989 by the engineer James Early. His design featured a glass shield constructed on the Moon and situated close to the first Lagrange point of the Sun-Earth system [7]. Since then, many have contributed to the idea in the form of conceptual suggestions and studies of practicality. Astronomer Roger Angel proposed in 2006 that the sunshade could be comprised of an assembly of small spacecrafts, all constructed on Earth and thereafter transported to the first Lagrange point, where they would form a sunshade constellation [8].

Assuming a sunshade constellation similar to the one suggested by Angel, the natural ensuing question is then how large the system would need to be. The total, combined size of the shade would depend on how much solar radiation needs to be reduced by as well as the system's distance from Earth. As for how much radiation shielding would be necessary in order to meet the goals of the Paris Agreement, it has been assessed that in order to fully mitigate a theoretical doubling of the amount of carbon dioxide in the atmosphere the shade system would need to block 1.7 % of solar radiation [9]. From this, C. Fuglesang and M. G. de Herreros Miciano [5] suggested the size of the sunshade system should be scaled to shield 1 % of incident solar radiation, and that this could reduce the temperature increase by 1 °C.

#### 2.1.2 Choice of propulsion system

Although remarkable similarities exist between solar sails and sunshades, as argued in reference [5], the former is relatively new in space technology and would require a large amount of prior research and testing. A more realistic approach in near future is to make

use of existing electric propulsion engines to raise satellites' orbit. Electric propulsion is more suitable in a low Earth orbit, as unexpected orbital maneuvers may take place in order to avoid possible collisions with other satellites or space debris. This is one of the advantages of electric propulsion over the solar sail, as it allows the spacecraft to vary the direction of the thrust without changing its magnitude. Assuming individual sunshades are first deployed outside of Earth's influence, solar sailing can then be used for further travel to the final position. This requires each sunshade to be fully equipped with both propulsion systems. Another option is to use electric propulsion all the way to the final destination and only unfolding the sunshades once they are in place. The solar sails are presumed to be used for station-keeping upon arrival in both cases.

### 2.1.3 Solar sailing in numbers

The first Lagrange point  $L_1$  in the Sun-Earth system is located at  $1.5 \cdot 10^6$  km measured from the Earth, equating to 0.01 astronomical units (AU). However the solar radiation pressure (SRP) displaces this point to a so called sub-Lagrange point  $L'_1$ , and the magnitude of this shift depends on the spacecraft's mass as well as the sail's optical properties. The equilibrium point corresponding to the minimal mass of the system was determined in [5], [6] to be located at  $2.36 \cdot 10^6$  km (corresponding to 0.0158 AU) from Earth, where the total shade area needed to reduce the amount of sunlight by 1% would be  $3.79 \cdot 10^{12}$  m<sup>2</sup>.

The sail's optical properties are encapsulated in the sail efficiency factor  $Q$ . There is a relationship between the sail efficiency, the areal density  $\rho_A$  and lightness parameter  $\beta$ , and the  $Q$ -factor thus affects both the acceleration during solar sailing but also the total mass at the equilibrium point. For solar sailing a high  $Q$  value is preferable, and the highest that was deemed possible was  $Q = 0.85$ . Once in place each spacecraft would rotate and face the sun with a low  $Q$  value, and state-of-the-art materials currently permits  $Q = 0.5$  but it was proposed that future development could admit as low as  $Q = 0.2$ . The lightness parameter used on the low  $Q$  side was  $\beta = 0.035$ . For the minimum mass point these values had corresponding areal densities  $\rho_A$  which grants balance of the forces. For the former, higher  $Q$ -value then this density was 21.9 g/m<sup>2</sup> while the latter value had 8.8 g/m<sup>2</sup>. At the same time the sail itself was estimated to have a density of 4 g/m<sup>2</sup> while the subsystems totaled 44 kg. In order to achieve the corresponding areal densities the area of the sail was adjusted. For  $Q = 0.5$  then this area was 2500 m<sup>2</sup> and the final mass (subsystems and sail) became 55 kg per sailcraft, while for  $Q = 0.2$  the area was 9000 m<sup>2</sup> with a mass of 81 kg. This means that in order to achieve the total shade area then  $1.5 \cdot 10^9$  sailcrafts would be needed for  $Q = 0.5$  corresponding to a grand total mass of  $8.3 \cdot 10^{10}$  kg, and  $4.2 \cdot 10^8$  sailcrafts with a combined mass  $3.4 \cdot 10^{10}$  kg for  $Q = 0.2$ . The study assumed a future launch-to-LEO cost of 50 US dollars per kilogram, and so the program would fetch a launch cost of  $1.7 - 4.2 \cdot 10^{12}$  US\$.

The sailcrafts' trajectories was divided into two parts, the escape from the Earth and then traversal to the sub-Lagrange point. With low  $Q$  side of  $Q = 0.5$  the first part took 531 day and the second an additional 72 days. For  $Q = 0.2$  the respective times were 285 days plus 88 days. For both cases the high  $Q$  side had the same value at  $Q = 0.85$ . It should be noted that it was assumed that the sail could have an optimal orientation at all times during the transfers, an idealisation which means that the real travel time

for the sail - especially during the escape from Earth - could be much longer.

Out of these two trajectory segments the escape from Earth was deemed the most risky and critical, as it crosses areas with increased accumulation of space debris. This debris poses a significant risk to the sailcraft's integrity and its future performance, since the large sails could easily be damaged. It was suggested to use chemical rockets to inject the sailcrafts directly into the escape trajectory as an alternative, however this study will investigate the possibility of using electrical propulsion for this purpose instead. In addition, since each sailcraft is encumbered by the additional weight of the thruster and accompanying power systems the second part of trajectory could be carried out via electric propulsion as well, in which case the sails would only need to act as shades and not as means of propulsion.

## 2.2 Electric propulsion

This section aims to provide a brief overview of electrical propulsion, its key types, features and advantages, as well as its most essential parameters. At the end of the section the specifications of current thruster designs are presented and some examples of missions which have successfully used electrical thrusters as the main propulsion system are given.

### 2.2.1 Ideal rocket equation

The mass of a spacecraft is often referred to as dry mass and wet mass. Dry mass includes all structural components as well as the payload mass - the mass of what the mission aims to deliver to the designated position. Wet mass is the dry mass plus the mass of the fuel and propellant which will be consumed during the mission. The system enclosing a spacecraft therefore has a time-dependent mass. During a short time interval  $\Delta t$  the small mass  $\Delta m$  is expelled with an exhaust velocity  $u$  relative to the spacecraft, causing the spacecraft to gain the velocity  $\Delta v$ . Observing the conservation of momentum and assuming external forces are null then yields

$$\begin{aligned} (m - \Delta m)(v + \Delta v) + \Delta m(v + \Delta v - u) &= mv \\ \implies m\Delta v &= u\Delta m \end{aligned} \tag{2.1}$$

By dividing equation (2.1) with  $\Delta t$  and using  $\lim_{\Delta t \rightarrow 0} \frac{\Delta v}{\Delta t} = \dot{v}$  and  $\lim_{\Delta t \rightarrow 0} \frac{\Delta m}{\Delta t} = -\dot{m}$  since the mass is reduced, it then follows

$$\dot{v} = -u \frac{\dot{m}}{m} = -I_{sp}g \frac{\dot{m}}{m} \tag{2.2}$$

where the specific impulse  $I_{sp} = \frac{u}{g}$  (with  $g$  as Earth's standard gravitational acceleration) is introduced in the last step and the term  $\dot{m}u = \dot{m}I_{sp}g$  is the spacecraft's thrust. The specific impulse is assumed constant, and integration of equation (2.2) thus gives

$$\Delta v = I_{sp}g \ln \left( \frac{m_0}{m_f} \right) \tag{2.3}$$

$$\frac{m_0}{m_f} = e^{\Delta v / I_{sp}g} \tag{2.4}$$

[10, p.212-214]. Equation (2.3) is also known as the Tsiolkovsky rocket equation, after the Russian rocket scientist Konstantin Tsiolkovsky who first derived it in 1903. The change in velocity  $\Delta v$  is ubiquitous in many spaceflight applications and commonly referred to as simply "delta-V".

## 2.2.2 Types of electric propulsion thrusters and how they work

Rockets used to launch from Earth's surface use chemical propulsion. This type of propulsion creates thrust through the expansion of gases produced from chemical reactions, which means the the expulsion velocity is limited by the energy in the chemical bonds. The specific impulse is a measurement of how fast the propellant is ejected out of the thruster and how efficiently the propellant is transformed into momentum. For a chemical rocket the propellant is ejected out at lower speeds, giving a subsequent lower specific impulse. However the thrust-to-weight ratio for this type of rocket is high and as a result the chemical rocket is a suitable choice in order to achieve lift-off from the surface of Earth.

Electric propulsion, often referred to as ion propulsion, uses electromagnetic fields to accelerate ions to very high velocities which gives a high specific impulse. Consequently this type of propulsion uses much less propellant for the same delta-V, and thus attains a better mass ratio equation (2.4), which permits an increase in payload mass. Albeit the velocity increase is achieved over a much longer period of time compared to chemical propulsion. The thrust produced is also relatively small due to electrical power constraints, and electric propulsion is therefore better suited for use in orbit (such as for station-keeping) or for interplanetary spaceflight.

There are three major types of electric propulsion - electrostatic, electromagnetic, electrothermal [11, p.3-5]. These are grouped according to the method of acceleration:

1. For electrostatic propulsion, an electric field is applied in the same direction as the desired acceleration, creating a Coulomb force acting on the ions. Two examples of electrostatic thrusters are the gridded ion thruster and the Hall thruster, and these designs can produce a specific impulse in the range of 1000 - 4000 s.
2. In electromagnetic propulsion the force is created by the use of electrical currents and magnetic fields, the latter being responsible for the acceleration. This type of propulsion has shown itself to be more difficult to implement, and as a result the technological development has been limited. The Pulsed Plasma Thruster is an electromagnetic thruster with successful missions in space, and a promising candidate is the Magnetoplasmadynamic (MPD) thruster which has been shown to produce an  $I_{sp}$  up to 10 000 s [12].
3. Lastly electrothermal propulsion creates thrust by electrical heating of the propellant. This causes thermal expansion and gas expulsion directed through a nozzle, much like in chemical propulsion. Thrusters such as the Arcjet and Resistojet are electrothermal, but since the heating of the propellant is limited consequently so is the exhaust velocity, and the specific impulse is low compared to the other two types - usually in the range of 500 - 700 s.

### 2.2.3 Parameters of electric propulsion thrusters

The performance of the thruster hinges on the utilization efficiency of the ionization process. The propellant can only be accelerated and provide thrust when it has been transformed into plasma, and more thrust is achieved when the process admits a high ratio between the exhaust flow rate of the ionized propellant  $\dot{m}_i$  and the propellant flow rate  $\dot{m}$  into the plasma generation chamber. For practical purposes the utilization efficiency is not ideal since it is difficult to measure accurately. A quantity more easily determined is the thrust  $T$ . Therefore the thrust efficiency  $\eta$  is more commonly used, and it is defined by

$$\eta = \frac{\dot{m}u^2}{2P} = \frac{(T^2)/\dot{m}}{2P} \quad (2.5)$$

where  $P$  is the available electrical power. The maximum value of  $\eta$  is 1.

A phenomenon called the *power supply mass penalty* becomes more noticeable with increasing exhaust velocity  $u$ . This entails a decrease of thrust per unit of supplied electrical power as the specific impulse is made higher, regardless whether the thrust efficiency is maximal. The effect is revealed by the thrust-to-power ratio

$$\frac{T}{P} = \frac{\dot{m}u}{\dot{m}u^2/2\eta} = \frac{2\eta}{u} = \frac{2\eta}{I_{sp}g} \quad (2.6)$$

The thrust-to-power ratio shows just why thrusters operating with electrical propulsion and high exhaust velocities produce low thrust, and how the thrust is limited by the available electrical power [13, p.4].

From equation (2.6) the acceleration which the thruster provides can be identified as

$$a_T = \frac{1}{m}T = \frac{2\eta P}{mI_{sp}g} \quad (2.7)$$

and its corresponding propellant flow rate

$$\dot{m} = \frac{T}{I_{sp}g} = \frac{2\eta P}{I_{sp}^2g^2} \quad (2.8)$$

### 2.2.4 Power sources and solar cells

The strength of the electromagnetic fields inside the thruster is limited by the available power, which needs to be generated aboard the spacecraft itself. This can be done through solar panels, batteries, or nuclear devices such as nuclear batteries or nuclear reactors.

Solar panels coupled with rechargeable batteries is by far the most prevalent choice of power generation (around 85 % of electrically driven spacecrafts use solar panels as of 2021) [14, section 3.2.1]. The reason for this is that they are readily available, produce reasonable power, and are comparably light-weight. However they have a few critical drawbacks, such as a high degradation rate caused by radiation and aging as well as their diminished efficiency proportional to  $\frac{1}{r^2}$  (where  $r$  is the distance to the Sun). The latter makes solar panels a less ideal choice for missions to planets far away in the Solar System [13, p.4].

Nuclear devices such as an RTG (radioisotope thermoelectric generator) or on board nuclear fission reactors are viable options which do not depend on solar power. The RTG is a nuclear battery which utilises the heat from radioactive decay to generate electricity. This technology exhibits high reliability and predictability in power production as well as a long lifetime, making it a good alternative for far-reaching space probes and has been demonstrated on for example the Cassini mission to Saturn and the New Horizons mission to Pluto [14, section 3.3.5] .

A spacecraft in the vicinity of the Sun benefits from the use of solar panels as their source of power generation. If electric propulsion was to be used to transfer the sunshades to the sub-Lagrange point then this is the most feasible alternative. In Table 2.1 there is a selection of solar panels either currently available or under development by spacecraft manufacturers [14, section 3.2.2].

*Table 2.1: A selection of solar panels developed for spacecraft power generation [14, section 3.2.2]. TRL denotes Technology Readiness Level.*

Solar cells			
Manufacturer	Model	Specific Power	TRL
Airbus Defense and Space	Sparkwing	165 W/kg	5-6
Exoterra	Fold Out Solar Arrays	140 W/kg	5-6
MMA Design	Hawk	121 W/kg	7-9
Agencia Espacial Civil Ecuatoriana	DSA/1A	107 W/kg	7-9
Redwire Space	ROSA	100 W/kg	5

## 2.2.5 Propellants

The choice of propellant not only affects the cost of the mission, but also the lifetime, efficiency and specific impulse of the thruster. A propellant with a higher mass gives a higher thrust efficiency and thus a better thrust-to-power ratio, as less of it needs to be ionized to attain the same level of thrust. Similarly, less power is needed for propellants with a low ionization potential - the energy required for ionization - but a high ionization cross section - the probability of ionization occurring. For practical purposes the propellant should be non-reactive, non-toxic and easy to store [15].

Many current designs of electric thrusters use xenon-propellant, but some alternatives are krypton, bismuth and iodine. Despite its high cost xenon is often favored since it has a high storage density and because of its properties as a noble gas - reactions with component's surfaces are mainly limited to sputtering. Krypton is somewhat less costly and can often be used almost interchangeably with xenon while still generating a high specific impulse. Its main disadvantages are that it has a lower storage density and yields a lower thrust efficiency. Bismuth is cheap, gives a high thrust efficiency and thrust-to-power ratio, and has an even higher storage density than xenon. However, since it is solid at STP the system needs to divert power to maintain a high temperature. Iodine is highly reactive, but works well at relatively low temperatures. It has a higher storage density than xenon and a comparable thrust efficiency, with a cost comparable to bismuth [13,

p.22].

## 2.2.6 Current electric propulsion thrusters

One reason to consider electric thrusters for the sunshade mission is the maturity as a technology compared to solar sailing. Electric thrusters have already been used as the primary propulsion system in numerous successful missions. The first spacecraft with an ion engine was the Deep Space 1, which in 1998 carried out consecutive fly-bys of the asteroid 9969 Braille and comet Borrelly [16]. Smart-1 was launched in 2003 and was the first Moon mission by the European Space Agency, and the satellite was injected into Geostationary-orbit via chemical rockets and subsequently used its Hall thrusters to transfer into Moon orbit [17]. A mission currently underway is the NASA Double Asteroid Redirection Test (DART). The aim is to test techniques to change the motion of an asteroid preventing its impact on Earth, and the propulsion system used is the gridded ion thruster NEXT-C. DART was launched in late 2021 and is expected to reach its target in September 2022 [18].

The choice of thruster is explored in this study, and the benefits of low propellant consumption from higher values of  $I_{sp}$  as well as higher thrust is weighed against the additional dry mass required to supply the required power. Some examples of electric propulsion thruster designs and their specifications are detailed in Table 2.2.

Table 2.2: Electrical thrusters either currently available or under development.

Electrical propulsion systems					
Name	Type	$I_{sp}$	Thrust	Efficiency	at Power
NSTAR [19]	Ion grid	$\sim 3200$ s	$\sim 90$ mN	0.61	2.3 kW
NEXT [20]	Ion grid	$\sim 4090$ s	$\sim 237$ mN	0.70	6.8 kW
T6 [21]	Ion grid	$\sim 4120$ s	$\sim 143$ mN	0.64	4.5 kW
XR-5 [22]	Hall	$\sim 1970$ s	$\sim 251$ mN	0.53	4.5 kW
BPT-4000 [23]	Hall	$\sim 2020$ s	$\sim 253$ mN	0.57	4.5 kW
AEPS [24]	Hall	$\sim 2600$ s	$\sim 589$ mN	0.57	13.5 kW
X3 [25]	Hall	$\sim 2340$ s	$\sim 5.42$ N	0.63	98.4 kW
Vasimir [26]	Electrothermal	$\sim 5000$ s	$\sim 6$ N	0.73	200 kW

## 2.3 Orbital mechanics

In this section, we aim to study orbital mechanics in order to compute the trajectory for a spacecraft from Earth to one of the Lagrange points in the Sun-Earth system. The models studied are the planar two body problem and the restricted three-body problem, with the critical acceleration provided by ion engines for an orbit transfer from LEO to escape as well as the final point on the Sun-Earth line.

### 2.3.1 Two-body problem

All equations presented in this section can be found in [27, p.35-37]. The two-body problem is a special case of the n-body problem and assumes only two objects in the

system. Other assumptions made for the two-body dynamics are:

- (i) The large body is spherical and its mass is evenly distributed, which means that its gravitational pull can be modeled as originating in its geometric center.
- (ii) The small body does not influence the large body gravitationally.

Let the vectors  $\vec{r}_1$  and  $\vec{r}_2$  represent the position of the two bodies whose masses are  $m_1$  and  $m_2$  with respect to an inertial reference frame. The distance between the two bodies is given by the radius vector  $\vec{r}$  (as depicted in Figure 2.1)

$$\vec{r} = \vec{r}_2 - \vec{r}_1 \quad (2.9)$$

By applying the Newton's gravitational, the second time derivative of equation (2.9) gives

$$\begin{aligned} \ddot{\vec{r}} &= \ddot{\vec{r}}_2 - \ddot{\vec{r}}_1 \\ &= \frac{\vec{F}_2}{m_2} - \frac{\vec{F}_1}{m_1} \\ &= \frac{1}{m_2} \left( \frac{Gm_1m_2}{r^3} \right) (-\vec{r}) - \frac{1}{m_1} \left( \frac{Gm_1m_2}{r^3} \right) \vec{r} \\ &= \frac{-G(m_1 + m_2)}{r^3} \vec{r} \\ &= -\frac{\mu_G}{r^3} \vec{r} \end{aligned}$$

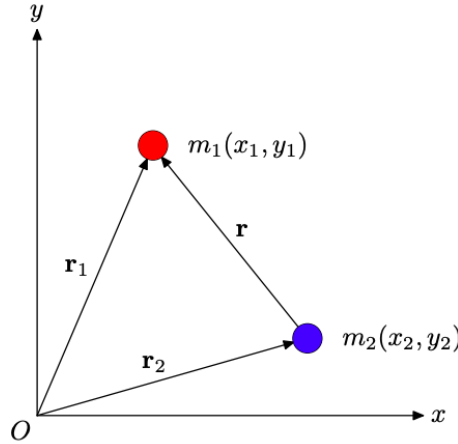


Figure 2.1: Two-body geometry. Credit [28]

where  $\mu_G = G(m_1 + m_2)$  and  $G$  is the Newtonian constant of gravitation  $G = 6.674 \cdot 10^{-11} Nm^2(Kg)^{-2}$ . However in the scenario of a spacecraft orbiting around a planet then the mass  $m_1$  is much greater than  $m_2$ , and the value  $\mu_G$  can be approximated by  $\mu_G \approx Gm_1$ . Furthermore, if there exists an arbitrary perturbation force  $\vec{F}$  acting on the mass  $m_2$  the equation of motion becomes

$$\ddot{\vec{r}} + \frac{\mu_G}{r^3} \vec{r} = \frac{\vec{F}}{m_2} \quad (2.10)$$

The perturbation force is in fact all the forces between the Earth and spacecraft that might perturb the spacecraft orbit. These forces can be the thrust generated by the spacecraft, solar radiation pressure, or gravitational influence of other planets. In order to find the trajectory for the spacecraft equation (2.10) needs to be solved numerically.

Let us consider the Earth, which is assumed to be fixed, and a satellite. An Earth centered inertial coordinate system (ECI) is considered, the origin of which lies at the center of the Earth, and so the  $\vec{r}_1$  is the zero vector. The basis vectors are  $\hat{x}$ ,  $\hat{y}$  and  $\hat{z}$ , where  $\hat{x}$  points towards the vernal equinox,  $\hat{z}$  towards the north pole, and  $\hat{y}$  defined to form the proper right handed coordinate system. In order to place a spacecraft into the desired orbit the engines need to produce thrust, which is one of the perturbations of the two-body problem. The following parameters can be introduced in a Cartesian frame:

$$\begin{aligned}\vec{r} &= (x, y) \quad \text{position vector} \\ \vec{v} &= \dot{\vec{r}} = (\dot{x}, \dot{y}) \quad \text{velocity vector}\end{aligned}\tag{2.11}$$

The perturbed equation (2.10) of satellite motion in Cartesian coordinates is then

$$\begin{aligned}\frac{d\dot{x}}{dt} &= \ddot{x}, & \ddot{x} &= -\frac{\mu_G}{r^3}x + \frac{F_x}{m_2} \\ \frac{d\dot{y}}{dt} &= \ddot{y}, & \ddot{y} &= -\frac{\mu_G}{r^3}y + \frac{F_y}{m_2}\end{aligned}\tag{2.12}$$

### 2.3.2 Low-thrust orbit transfer and delta-V budget

When Earth's gravity is the dominating factor the system can be modeled as a two-body problem. The thrust produced by ion engines is many orders of magnitude smaller than the gravitational force, which affects how the transfer between orbits is carried out.

Starting from equation (2.10) and assuming external forces are null, the total energy per unit of mass for a satellite in orbit around a celestial body can be derived. This is called the specific orbital energy and is written as

$$\mathcal{E}_{orb} = \frac{v^2}{2} - \frac{\mu_G}{r} = -\frac{\mu_G}{2a}\tag{2.13}$$

where  $v = \|\vec{v}\|$  is the orbital speed of the satellite relative to the body,  $r$  is the radial distance between the satellite and the body's center of mass, and  $a$  is the semi-major axis of the orbit [10, p.54-60]. In particular,  $\mu_G$  is approximately equal to the Earth's standard gravitational parameter and thus more or less constant. The rate of increase in orbital energy is

$$\dot{\mathcal{E}}_{orb} = \frac{\mu_G}{2a^2}\dot{a}\tag{2.14}$$

and the work performed by the propulsion system has a rate of

$$\dot{\mathcal{E}}_{orb} = \frac{1}{m}\vec{F} \cdot \vec{v}\tag{2.15}$$

When the thrust is limited the rate of increase in orbital energy is maximised when the force and velocity vectors are parallel, according to equation (2.15). This means that minimal propellant is used when the thrust is tangential to the orbit and the trajectory then becomes an outward spiral.

Assuming the acceleration is small and the orbit approximately circular, then the speed of the satellite can be estimated as  $v^2 \approx \frac{\mu_G}{a}$ . Using this in equation (2.15) along with equation (2.14) yields a separable differential equation in  $a$  and  $t$ . The solution to this equation is

$$\frac{1}{\sqrt{a_0}} - \frac{1}{\sqrt{a_f}} = \frac{F}{m\sqrt{\mu_G}}(t_0 - t_f)$$

Rearranging then gives

$$\Delta t = \frac{m\sqrt{\mu_G}}{F} \left( \frac{1}{\sqrt{a_0}} - \frac{1}{\sqrt{a_f}} \right) \quad (2.16)$$

$$t_{esc} = \frac{m}{F} \sqrt{\frac{\mu_G}{a_0}} \quad (2.17)$$

for the time required to transfer between an orbit with semi-major axis  $a_0$  to  $a_f$ , time for escape  $t_{esc}$  where the orbit is parabolic ( $a_f \rightarrow \infty$ ) [10, p.98-99].

Additionally, defining escape from Earth as the point when specific orbital energy goes from negative to zero, equation (2.13) can be used to solve for the final speed as a function of radial distance  $r$  to Earth's center

$$v_{esc} = \sqrt{\frac{2\mu_G}{r}} \quad (2.18)$$

Equation (2.18) defines the escape velocity for a spacecraft. When the spacecraft has escaped Earth and is more substantially affected by the gravitational force from the Sun, the system is modeled as a three-body-problem.

### 2.3.3 The restricted three body problem

The restricted problem of three bodies describes the motion of a third body with negligible mass in a rotating coordinate system. The two revolving bodies are called the primaries and their motion is approximated as circular Keplerian orbits around their center of mass (barycenter). The third body is influenced by the gravitational pull of the primaries, and we are concerned with the system composed of the two primaries Sun-Earth and a spacecraft. The spacecraft is in a rotating frame and the two primaries are fixed on the x-axis. It then moves in a gravitational potential field that rotates uniformly with respect to the inertial reference frame. The dependent variables,  $x$  and  $y$ , refer to the rotating system.

The equations of motion for the third body are derived comprehensively in [29, p.7-22], and the essential points are summarised below.

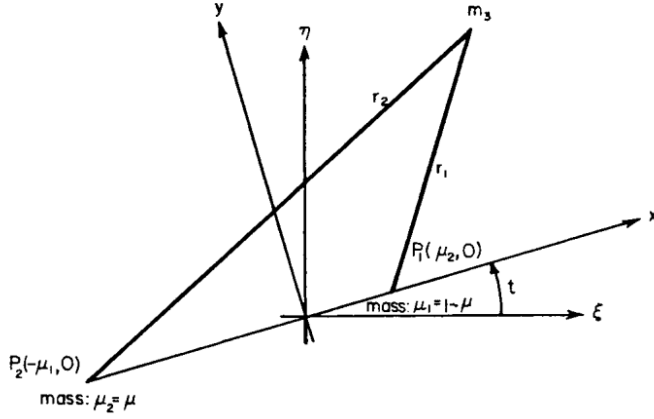


Figure 2.2: Notation for the dimensionless rotating system  $(x, y)$  where the larger mass  $1-\mu$  is placed to the right of the origin. Credit [29, p.20]

For the restricted problem of three bodies, a dimensionless system of variables is used. This means that:

- (i) The distance between the primaries is unity.
- (ii) The angular velocity ( $\Omega$ ) of the motion of  $M_1$  and  $M_2$  is assumed to be one.
- (iii) The mass of the smaller primary  $M_2$  is given by the mass ratio  $\mu = \frac{M_2}{M_1+M_2}$  and the mass of primary  $M_1$  is given by  $(1-\mu)$ , so the total mass of the system is also one.
- (iv) The position of the two primaries in non-dimensional units are then  $(\mu, 0)$  and  $(-1+\mu, 0)$  for the larger and the smaller primary respectively (see Figure 2.2). The position of the third body is denoted by  $(x, y)$ .
- (v) The unit of time is defined such that the period of the motion of the primaries is  $2\pi$ .
- (vi) The gravitational constant,  $G$ , becomes one.

The equations of motion in the x-y-plane for the third body are then

$$\begin{aligned} \ddot{x} - 2\dot{y} &= \frac{\partial U}{\partial x} \\ \ddot{y} + 2\dot{x} &= \frac{\partial U}{\partial y} \end{aligned} \tag{2.19}$$

where dots denotes derivatives with respect to the dimensionless time  $\tau$ , and  $U$  is the linear sum of the gravitational and the centrifugal potential. It is also sometimes referred to as the pseudo-potential, and given by

$$U(x, y) = \frac{x^2 + y^2}{2} + \frac{1 - \mu}{r_1} + \frac{\mu}{r_2} \tag{2.20}$$

where  $r_1$  denotes the distance between the spacecraft and the first primary and likewise  $r_2$  denotes the distance between the spacecraft and the second primary.

$$\begin{aligned} r_1 &= \sqrt{(x - \mu)^2 + y^2} \\ r_2 &= \sqrt{(x + 1 - \mu)^2 + y^2} \end{aligned} \tag{2.21}$$

This system of equations has no analytical solutions. In order to find optimal trajectories in the three-body problem when the third body is a spacecraft, optimal control must be used to find the thrust directions and magnitudes.

### 2.3.4 Sun-Earth Lagrange points

Lagrange points are equilibrium points for a third body of negligible mass under the influence of two massive orbiting bodies. At these positions in the Circular Restricted Three Body Problem (CRTBP), the resultant gravitational force due to two large bodies must be equal to the centripetal acceleration necessary to keep the object in orbit at that particular distance from the larger primary, with the same angular velocity as that of the two main bodies around their common center of mass [30, p.2]. In the Sun-Earth-system, the center-of-mass lies inside the Sun and as a result there is a slight wobble in the motion of the Sun in comparison to the motion of the Earth around the barycenter. Therefore, assuming the Sun is stationary, the angular velocity of a spacecraft placed at the liberation points coincides with the angular velocity of the Earth around the Sun. There are five points of equilibrium between any two body system, which means that a spacecraft located at one of these points with zero velocity and acceleration will remain there indefinitely. The first three points,  $L_1$ ,  $L_2$  and  $L_3$  are unstable and hence the slightest disturbance to any object located at one of them causes the object to drift away. The triangular points ( $L_4$  and  $L_5$ ) as shown in Figure 2.3 are stable in the Sun-Earth system. The unstable points require a small amount of delta-V for station-keeping, in the form of regular thruster firings [31].

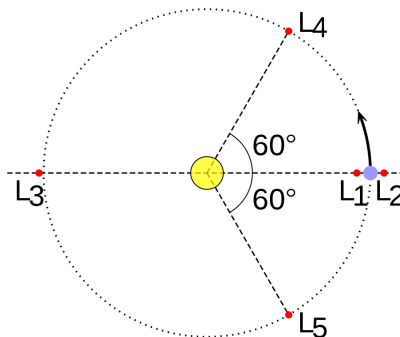


Figure 2.3: Illustration of the five Lagrange points between Sun-Earth-system. Credit [32]

### 2.3.5 Solar pressure and sub-Lagrange point

The preferred location for the sunshade configuration is a point in the vicinity of the  $L_1$  liberation point where the gravitational forces from the Sun and Earth together with the solar radiation pressure (SRP) balance in the CRTBP reference frame. If SRP is

not considered, the equilibrium position corresponds to the classic  $L_1$  which is located at  $1.5 \cdot 10^6$  km from the Earth. However, the large surface meant to shade Earth also gives rise to a non-negligible amount of SRP directed away from the Sun. Due to the additional SRP acceleration, three-body dynamics allow for an infinite number of artificial equilibrium points, so called sub-Lagrange points  $L'_1$ , between the Sun and the classic  $L_1$  [33, p.217-218]. There exists a minimum mass equilibrium point for the system, and this is positioned sunwards and therefore further away from Earth compared to the classic first-Lagrange point.

The radius  $R_{disk}$  of a circular sunshade configuration at a distance  $d_{disk}$  from the Earth and a solar flux ratio  $\Delta S/S$  are related by

$$R_{disk} = R_{\odot} \frac{d_{Disk}}{d_{\odot}} \sqrt{\frac{\Delta S}{S}} \quad (2.22)$$

where  $R_{\odot}$  is the radius of the Sun,  $d_{Disk}$  is the distance of the sunshades from Earth,  $d_{\odot}$  is the distance of the Sun to Earth,  $S$  is the total solar flux received at the Earth and equal to  $1367 \text{ W/m}^2$ , and finally  $\Delta S$  is the amount of solar flux that is to be absorbed by the sailcraft [34]. The ratio  $\Delta S/S$  used in this thesis is 1 %. At the classical Sun-Earth Lagrange  $L_1$  point, which lies at a distance of  $1.5 \cdot 10^6$  km from Earth, a solar disk radius  $R_{disk}$  of 696 km or a structure with an equivalent area of  $1.5 \cdot 10^{12} \text{ m}^2$  would be required. However, this position is infeasible as solar radiation pressure moves the equilibrium point towards the Sun.

The most costly feature of the sunshade project is the total mass launched from Earth, and to minimise launch costs the mass to offset the SRP should then be minimized. This mass tends to infinity at the classical  $L_1$  position and also increases if the sunshade configuration is placed closer to the Sun, since more area would be required for the same amount of  $\Delta S$ . The optimal mass position is a minimum mass point located close to  $2.36 \cdot 10^6$  km from Earth [6]. The total shade area required at this distance for the 1 % goal is given by equation (2.22), resulting in  $3.79 \cdot 10^{12} \text{ m}^2$ .

As previously stated, at any equilibrium point the external acceleration of a sailcraft due to SRP and gravitational influence of the Earth and Sun must equal the centripetal acceleration needed to keep the sunshade in an orbit around the Sun. The acceleration of the sunshades depends on the reflectivity and total mass of the system. Higher reflectivity gives a larger SRP force and leads to a larger displacement. A larger mass on the other hand is more affected by the gravitational forces. Consequently, a higher value of  $Q$  corresponds to a larger total mass of the sunshade project for the same minimum mass equilibrium point. The ideal case in the manufacturing of the sunshade project would be to attain the lowest  $Q$ -value possible as it will result in minimum total mass of the system.

# Chapter 3

## Investigation

### 3.1 Problem

The study will be performed for two cases: First by using electric propulsion for a partial trajectory only to escape the Earth's gravitational field and assuming solar sailing can be used for the remainder, and second by letting electric propulsion be the sole propulsion method for the full trajectory the sub-Lagrange point. The first case can be modeled entirely in a two-body system with an analytically derived, approximately optimal thrust direction. The latter must be solved using optimal control and the model used will be the Circular Restricted Three-Body Problem. This case in question was done in two sections, using the results from the two-body problem (with additional propellant mass) and transforming into a new coordinate system with the final values of this trajectory used as initial values in the three-body model.

#### 3.1.1 Optimal control problem

An optimal control problem is the task of finding the controls for a system which will optimise a specific quantity. The system is described by the state variables  $\vec{x}$  and the control variables  $\vec{u}$ , and the dynamics of it are enclosed in the state equations  $\dot{\vec{x}}(t)$ .  $J(\vec{x}, \vec{u})$  is the cost or objective function, and it is the quantity which is to be optimised. The restrictions on the variables in points along the trajectory are called the path constraints  $p(t, \vec{x}, \vec{u})$ , and the restrictions on the state variables at the initial and final points are called the boundary conditions  $b(t_0, t_f, \vec{x}_0, \vec{x}_f)$ .

In general the optimal control problem can be formulated as [35, p.13]:

$$\begin{aligned} J(\vec{x}, \vec{u}) &= H(t_0, t_f, \vec{x}_0, \vec{x}_f) + \int_{t_0}^{t_f} g(t, \vec{x}, \vec{u}) dt \\ \dot{\vec{x}}(t) &= f(t, \vec{x}, \vec{u}) \\ p(t, \vec{x}, \vec{u}) &\leq 0 \\ b(t_0, t_f, \vec{x}_0, \vec{x}_f) &\leq 0 \end{aligned}$$

where  $H, g, f$  are functions dependent on the problem in question,  $t_0$  denotes initial time and  $t_f$  the final time. For the specific case of this study, the state variables  $\vec{x}$  are the

position, velocity and mass of the satellite. The state equations are the differential equations derived from orbital dynamics, while the control variables  $\vec{u}$  are the thrust vector's components. The cost function depends on the aim of the mission, and can for example be chosen as either minimal use of propellant or minimal time required for the maneuver.

There are many ways of solving an optimal control problem, two of which are the indirect method and the direct method. The indirect methods are based on the Pontryagin's Maximum Principle derived from calculus of variations. To find the optimal control the problem is defined as Hamiltonian system and transformed into a boundary value problem (BVP). This resulting BVP can then be solved numerically or in some instances analytically in order to find the optimal control law for the system. Direct methods are based around transforming the optimal control problem into a non-linear programming problem via discretisation, which can then be solved with optimisation algorithms [35, p.18-24] .

This latter method was the one chosen for this project and details of implementation are given in section 3.4.2.

## 3.2 Model

### 3.2.1 Two body problem equations in polar coordinates

As suggested in [36], the equations of motion (2.12) were represented in polar coordinates together with (2.8), and thrust divided into its components. The system was rewritten to first-order with the variables:

$$\begin{aligned}\dot{r} &= v_r \\ \dot{\theta} &= \omega \\ \dot{v}_r &= \ddot{r} \\ \dot{\omega} &= \ddot{\theta}\end{aligned}$$

where  $r$  and  $\theta$  are the position coordinates of the two dimensional polar coordinate system,  $v_r$  is the radial velocity and  $r\omega$  the tangential velocity  $v_\theta$ . The second order derivatives represents the acceleration of the spacecraft. With the new variables then the state equations are given by

$$\dot{\vec{x}} = \begin{bmatrix} \dot{r} \\ \dot{\theta} \\ \dot{v}_r \\ \dot{\omega} \\ \dot{m} \end{bmatrix} = \begin{bmatrix} v_r \\ \omega \\ r\omega^2 - \frac{\mu_G}{r^2} + \frac{1}{m}T_r \\ \frac{-2v_r\omega}{r} + \frac{1}{rm}T_\theta \\ \frac{-T}{I_{sp}g} \end{bmatrix} \quad (3.1)$$

Here the thrust vector in polar coordinates is  $\vec{T} = [T_r, T_\theta]$  and  $T = \|\vec{T}\|$ . As explained in section 2.3.2, the approximately optimal direction of this vector for minimal use of propellant is tangential. Therefore the thrust was modeled as continuous with  $\vec{T} = [0, T_{max}]$

and the system could then be solved through numerical integration.

The initial condition for the state variables is the state of the spacecraft in LEO shortly after the payload fairing of the chemical rocket has been jettisoned. The initial radius  $r(t_0) = r_0$  is the sum of Earth's average radius and the altitude of LEO. The angular velocity  $\omega(t_0)$  can be approximated from the orbital velocity due to the centripetal force of the Earth ( $v_o = \sqrt{\frac{\mu_G}{r_0}}$ ). The radial velocity of the spacecraft and the initial angle  $\theta$  is assumed to be zero before thrust is applied.

$$\vec{x}(t_0) = \begin{bmatrix} r(t_0) \\ \theta(t_0) \\ v_r(t_0) \\ \omega(t_0) \\ m(t_0) \end{bmatrix} = \begin{bmatrix} r_0 \\ 0 \\ 0 \\ \omega_0 = \frac{1}{r_0} \sqrt{\frac{\mu_G}{r_0}} \\ m_0 \end{bmatrix} \quad (3.2)$$

The boundary condition at the final time is the specific orbital energy equation (2.13), which at the point of escape goes from negative to positive

$$\mathcal{E}_{orb} = \frac{v_r^2(t_f) + [r(t_f)\omega(t_f)]^2}{2} - \frac{\mu_G}{r(t_f)} = 0 \quad (3.3)$$

At this point the spacecraft is said to have escaped Earth and integration was stopped.

### 3.2.2 Characteristic Quantities and Nondimensionalisation in the Circular Restricted Three-Body Problem

The approach in this sections follows the examples set in [37], [38]. Dynamics of the CRTBP describe the motion of the spacecraft when it is placed in a synodic (co-rotating) coordinate system with the origin at the barycenter of the Sun-Earth-system. This coordinate system is illustrated in Figure 3.1, and the Sun lies on the right side of the origin as the barycenter is located closer to the larger mass.

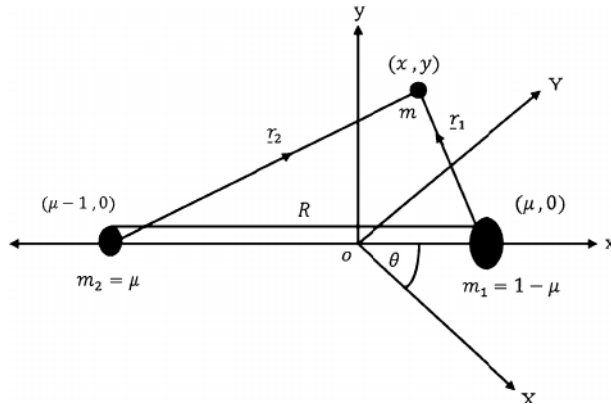


Figure 3.1: The synodic  $[x, y]$  coordinate system with the origin at the center-of-mass of the Sun-Earth-system. The  $[X, Y]$  coordinate system is inertial and in this case resembles an ecliptic coordinates system without translation of origins. Credit [39]

It follows that the location of each primary on the rotating x-axis in nondimensional units are  $(\mu, 0)$  and  $(\mu - 1, 0)$ . Change of coordinate systems from ECI to CR3BP will result in a z-coordinate for the spacecraft. Thus the dynamics of planar CRTBP equation (2.19) must be extended to further incorporate the third position coordinate

$$\begin{aligned}
\ddot{x} &= 2\dot{y} + x - \frac{(1-\mu)(x-\mu)}{r_1^3} - \frac{\mu(x+1-\mu)}{r_2^3} \\
\ddot{y} &= -2\dot{x} + y - \frac{(1-\mu)y}{r_1^3} - \frac{\mu y}{r_2^3} \\
\ddot{z} &= \frac{-(1-\mu)z}{r_1^3} - \frac{\mu z}{r_2^3} \\
r_1 &= \sqrt{(x-\mu)^2 + y^2 + z^2} \\
r_2 &= \sqrt{(x+1-\mu)^2 + y^2 + z^2}
\end{aligned} \tag{3.4}$$

where  $r_1$  once again denotes the position of the spacecraft relative to the Sun and similarly  $r_2$  the position of the spacecraft relative to Earth, as shown in Figure 3.1. Dynamics of the CRTBP are described in dimensionless units and thus characteristic units must be introduced for the Sun-Earth system specifically. The mass ratio between the Earth and Sun is defined as

$$\mu = \frac{m_{Earth}}{m_{Sun} + m_{Earth}} = 3.003481 \cdot 10^{-6} \tag{3.5}$$

To nondimensionalise, the characteristic quantities used for length, mass, time and thrust in the Sun-Earth system are

$$\begin{aligned}
\ell^* &= 1 \text{ AU} = 1.495979 \cdot 10^8 \text{ km} \\
m^* &= m_{Sun} + m_{Earth} = 1.988481 \cdot 10^{30} \text{ kg} \\
\tau^* &= \sqrt{\frac{(\ell^*)^3}{Gm^*}} = 58.13237 \text{ days} \\
v^* &= \frac{\ell^*}{\tau^*} = 29.785 \text{ km/s} \\
T^* &= \frac{\ell^* m_{satellite}}{(\tau^*)^2}
\end{aligned} \tag{3.6}$$

The characteristic time  $\tau^*$  is chosen such that the nondimensional gravitational constant  $G$  is equal to one. Escape velocities from the two-body problem can be nondimensionalised by dividing with  $v^*$ .

### 3.2.3 Coordinate systems

For the two-body problem, equations of motion were solved in the ECI system. This ECI coordinate system lies in the Earth's equatorial plane which does not coincide with Earth's orbital plane around the Sun. The orbital plane of the Earth is the ecliptic plane, and all the bodies in our Solar System lie in or close to this plane. For Earth the axis of rotation is tilted away by an angle known as the obliquity of the ecliptic,  $\varepsilon$ . On average,  $\varepsilon$  is  $23.45^\circ$ . The Earth's equatorial plane and the ecliptic intersect along a line, which is known as the vernal equinox line, at a specific time during the year. It is also known as the March equinox since it occurs between March 19 to 21 each year. The Earth's

equator is then declined by  $23.45^\circ$  with respect to the Earth's orbit plane around the Sun, and the declination leads to a negative  $\varepsilon$ .

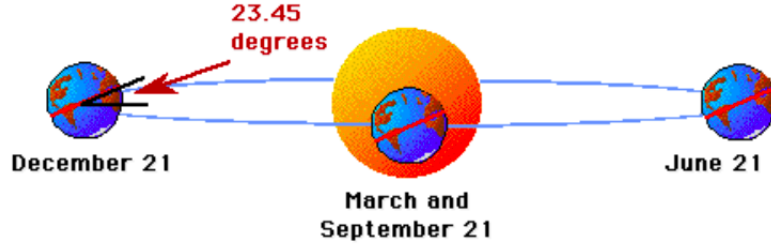


Figure 3.2: Illustration of the Earth's obliquity of the ecliptic relative to its motion around the Sun. The equatorial plane is tilted downwards with respect to the ecliptic plane by the angle  $\varepsilon$ . Credit [40]

The escape spiral transfer takes place entirely in the equatorial plane with the inertial ECI coordinate system, but the remaining trajectory will take place in the CR3BP coordinate system. Thus a transformation between these two systems must take place, and will be done in consecutive steps.

Taking into account Earth's tilt with respect to its ecliptic plane, a first transformation of position coordinates and velocities to the ecliptic plane must be performed. Next, a transformation from inertial Earth-centered to a rotating Earth-centered coordinate systems takes place, which accounts for the velocity difference between inertial and rotating systems. After which a simple translation of origin is needed in order to move from Earth-centered to a synodic coordinate system.

The various coordinate system transformations can be summarised as below.

- (i) Escape position coordinates can be transformed from polar coordinates to Cartesian coordinates using Matlab *pol2cart*. The escape velocity in Cartesian coordinates are given in equation (3.7) where spacecraft's escape position and velocity in polar coordinates are known as inputs:

$$\begin{aligned} v_x &= \dot{r} \cos \theta - r \dot{\theta} \sin \theta \\ v_y &= \dot{r} \sin \theta + r \dot{\theta} \cos \theta \end{aligned} \quad (3.7)$$

- (ii) A coordinate transformation from an equatorial to an ecliptic plane in the Earth-centered non-rotating reference frame takes place. As both systems are fixed, aligned along the vernal equinox, a simple projection from equatorial to the ecliptic plane using a rotation-matrix is needed for both position and velocity coordinates:

$$\begin{bmatrix} x_{ecliptic} \\ y_{ecliptic} \\ z_{ecliptic} \end{bmatrix} = \begin{bmatrix} 1 & 0 & 0 \\ 0 & \cos \varepsilon & -\sin \varepsilon \\ 0 & \sin \varepsilon & \cos \varepsilon \end{bmatrix} \begin{bmatrix} x_{equatorial} \\ y_{equatorial} \\ z_{equatorial} \end{bmatrix} \quad (3.8)$$

- (iii) Another coordinate-system transformation takes place from the ecliptic system to a rotating coordinate system with its origin in Earth's center, known as ECEF (Earth-centered - Earth-fixed). Position coordinates are not affected by this transformation, resulting in  $\vec{r}_{ECEF} = \vec{r}_{ecliptic}$ . For velocity transformation the angular velocity of Earth must be taken into account. The general formula for velocity transformation from an inertial to a rotating coordinate system is given in equation (3.9)

$$\vec{v}_{rot} = \vec{v}_{inertial} - \vec{\Omega} \times \vec{r} \quad (3.9)$$

For transformation of the escape velocities between ecliptic and ECEF then equation (3.9) translates to

$$\vec{v}_{esc, ECEF} = \vec{v}_{esc, ecliptic} - \vec{\Omega} \times \vec{r}_{esc, ecliptic} \quad (3.10)$$

where  $\Omega$  is the angular velocity of the Earth around the Sun, and therefore  $\Omega = 2\pi/(365 \cdot 24 \cdot 60 \cdot 60 \text{ s}) \approx 2 \cdot 10^{-7} \text{ rad/s}$ . In component form equation (3.10) becomes

$$\begin{aligned} v_{ECEF, x} &= v_{ecliptic, x} + \Omega \cdot y_{esc} \\ v_{ECEF, y} &= v_{ecliptic, y} - \Omega \cdot x_{esc} \\ v_{ECEF, z} &= v_{ecliptic, z} \end{aligned} \quad (3.11)$$

- (iv) Now is a good time to perform nondimensionalisation of positions and velocities before transformation to the CRTBP synodic coordinate system.

$$\begin{aligned} x_{nondim} &= \frac{x_{ecliptic}}{\ell^*}, & y_{nondim} &= \frac{y_{ecliptic}}{\ell^*}, & z_{nondim} &= \frac{z_{ecliptic}}{\ell^*} \\ v_{x,nondim} &= \frac{v_{x, ECEF}}{v^*}, & v_{y,nondim} &= \frac{v_{y, ECEF}}{v^*}, & v_{z,nondim} &= \frac{v_{z, ECEF}}{v^*} \end{aligned} \quad (3.12)$$

- (v) For transformation to the synodic coordinate system with its origin in the barycenter, position coordinates need only be translated in the  $\hat{x}$ -direction. The transformation between ECEF and the synodic coordinate system does not affect the velocities given in equation (3.12). In the synodic system  $\hat{x}$  lies along the vernal equinox which points from Earth towards the Sun. Translating origins from Earth-centered to barycenter:

$$x_{synodic} = x_{nondim} - (1 - \mu), \quad y_{synodic} = y_{nondim}, \quad z_{synodic} = z_{nondim} \quad (3.13)$$

### 3.2.4 Optimal control problem in three-body dynamics

For minimal fuel, with state equations (2.8) and (3.4), the optimal control problem was defined as

$$\mathbf{min} J = -m(t_f)$$

**Subject to**

$$\dot{\vec{x}} = f(\vec{x})$$

$$\vec{x} = \begin{bmatrix} x \\ y \\ z \\ \dot{x} \\ \dot{y} \\ \dot{z} \\ m \end{bmatrix} = \begin{bmatrix} x_1 \\ x_2 \\ x_3 \\ x_4 \\ x_5 \\ x_6 \\ x_7 \end{bmatrix}, \quad f(\vec{x}) = \begin{bmatrix} x_4 \\ x_5 \\ x_6 \\ 2x_5 + x_1 - \frac{(1-\mu)(x_1-\mu)}{r_1^3} - \frac{\mu(x_1+1-\mu)}{r_2^3} + \frac{u_x}{x_7} \\ -2x_4 + x_2 - \frac{(1-\mu)x_2}{r_1^3} - \frac{\mu x_2}{r_2^3} + \frac{u_y}{x_7} \\ -\frac{(1-\mu)x_3}{r_1^3} - \frac{\mu x_3}{r_2^3} + \frac{u_z}{x_7} \\ -\frac{\sqrt{u_x^2 + u_y^2 + u_z^2} \ell^*}{I_{sp} g_0 \tau^*} \end{bmatrix}$$

**Path constraints on control variables**  $u_x, u_y, u_z$

$$u_x^2 + u_y^2 + u_z^2 \leq f^2, \quad \text{where } f \text{ denotes maximal, nondimensional thrust magnitude}$$

**Path constraints on state variables**

$$m \geq m_{dry} \quad \forall t$$

**Boundary constraints**

$$x_0 = \text{Values at escape from Earth}$$

$$x_f = \text{Coordinates at } L'_1 \text{ and null velocities}$$

(3.14)

In the case of minimal time the system of equations and constraints are the same with the exception of the cost function

$$\mathbf{min} J = t_f$$

## 3.3 Analytical Calculations

### 3.3.1 Delta-V budget for ion propulsion

To determine how much propellant a spacecraft requires the maximum change in velocity, the delta-V, can be calculated. The total delta-V for a space mission is the linear sum of the delta-V needed to perform each propulsive maneuver needed during the mission. Starting at the surface of the Earth, a delta-V of around 9.4 kilometers per second is required to put a spacecraft into a low Earth orbit. A low Earth orbit (LEO) is an orbit around Earth with an altitude between 160 kilometers and 2000 kilometers. Most of this delta-V is lost to gravity, and roughly 1.3-1.8 km/s is lost to atmospheric drag [41]. This will put the spacecraft into LEO with an orbital velocity of around 7-8 km/s, but the value depends on the altitude in LEO ( $\sim \sqrt{\frac{1}{r}}$ ). In order to further escape Earth's gravity well the orbital velocity must go to zero, which will also be to the total delta-V needed to

escape Earth’s gravity. Chemical rockets are used as launching vehicles (because of their high thrust-to-weight ratio) starting from the surface of Earth. This gets the spacecrafts into LEO, after which the on-board low-thrust propulsion is used to attain Earth escape velocity.

A natural inquiry for this large-scale mission is to investigate what altitude in LEO the spacecraft should be launched into for minimal propellant costs. Objects below approximately 160 kilometers experience very rapid orbital decay and altitude loss [41]. If the sunshade project uses solar sails instead of electric propulsion an altitude above 1000 km is necessary to avoid atmospheric drag as well as low orbiting satellites. However, ion propulsion has demonstrated the ability to perform significant orbital maneuvers at lower altitudes [42] and it is therefore worthwhile to study different launch altitudes.

Electric propulsion is of great interest because of its inexpensive nature compared to conventional rockets, especially for a large scale mission design such as the sunshade project. It may be compelling to let the spacecraft use its own propellant from a low launch orbit, however at very low altitudes ( $\leq 300$  km) atmospheric drag poses a significant risk to spacecraft’s components and reduces their lifetime. Even for Earth orbiting satellites such as in reference [42], the initial launch altitude is approximately 600 km above the Earth’s surface and thereafter further altitude lowering orbital maneuvers are performed.

The escape trajectories in the two-body problem for very low thrust takes form of circular orbits that are successively raised from an initial launch orbit to an escape final orbit. The assumption that the orbits remains circular will break down as the spacecraft approaches escape speed. However, in the derivation for delta-V it is a useful approximation. For orbit raising, semimajor axis of the orbit  $a$  must be increased. The total energy per unit mass of the spacecraft and semimajor axis  $a$  are related by equation (2.13). By running similar calculations as in section 2.3.2 one can establish the equation for the time required to complete a given transfer as in equation (2.16) The total velocity change expected of the spacecraft will be the time the engines must run multiplied by the specific acceleration of the spacecraft, or

$$\Delta v_{esc} = \frac{F}{m} \Delta t \tag{3.15}$$

Substituting equation (2.16) into equation (3.15) yields an equation for delta-V required for a given orbit transfer in terms of initial and final semimajor axes of the escape orbit,

$$\Delta v_{esc} = \sqrt{\frac{\mu_G}{a_0}} - \sqrt{\frac{\mu_G}{a_f}} \tag{3.16}$$

As before, at escape radius the final semimajor axis  $a_f$  tends to infinity as the orbit becomes parabolic. However, numerically  $a_f$  has a finite value and denotes radius of Earth’s sphere of influence for the specific spacecraft. Consequently, numerical delta-V is less than delta-V presented here. The total delta-V required from an initial launch orbit to the escape radius ( $a_f \rightarrow \infty$ ) can be calculated as in equation (3.17) where  $R_{\oplus}$

denotes Earth radius and  $h$  represents initial altitude in LEO.

$$\Delta v_{esc} = \sqrt{\frac{\mu_G}{a_0}} = \sqrt{\frac{\mu_G}{R_{\oplus} + h}} \quad (3.17)$$

For calculating mass ratio between dry and propellant mass equation (2.4) is applied. Dry mass and  $I_{sp}$  values for the NEXT Thruster are the most suitable (see section 3.5.1).

*Table 3.1: Different altitudes for initial parking orbits and respective delta-V needed to escape for a dry mass of 240 kg.*

Delta-V for different parking orbits			
Altitude in LEO	Delta-V	$m_{prop}/m_0$	Propellant mass
600 km	7.559 km/s	17.2 %	49.7 kg
1400 km	7.160 km/s	16.3 %	46.8 kg
2000 km	6.898 km/s	15.8 %	44.9 kg

As expected delta-V and orbital velocity for an object at a lower altitude is higher, and as a result more propellant is required for escape (see Table 3.1). A single sunshade launched to a 600 km parking altitude requires approximately 5 kg more propellant for electric propulsion than one launched to an initial altitude of 2000 km. The small increase in propellant mass results in few extra days for the escape trajectory (section 3.5.2) although this may enhance the launcher’s payload capacity. The maximum payload for a launch vehicle is usually defined for an altitude of 500 km in LEO and it decreases for higher parking orbits. As a result, low parking orbits allow for fewer launches for the total payload, reducing launch costs considerably. However, higher parking orbits reduce the risk of collisions with near Earth satellite constellations as well as enabling less time spent in the Van Allen radiation belts.

If the spacecraft is to use electric propulsion as the sole source of propulsion, another thrust arc is required after escape in order for the spacecraft to reach the  $L'_1$  of the Sun-Earth system. Analytically there is no suitable equation for calculating delta-V required for this maneuver. The trajectory computation for such a transfer is most frequently done using optimal control in three-body dynamics.

## 3.4 Numerical Analysis

### 3.4.1 Two-body problem

The dynamics in equation (3.1) of the planar two body problem were propagated using numerical integration until the final condition equation (3.3) was met. The algorithm used was the explicit Runge-Kutta of order 4 (RK4) with a stepsize of  $h = 0.1$ .

Initial conditions equation (3.2) were set with  $r_0 = 8.371 \cdot 10^6$  (using an altitude of 600-2000 km in LEO),  $\mu_G = 3.986 \cdot 10^{14}$ , and  $m_0$  varied depending on thruster and its specific impulse.

### 3.4.2 Three-body problem

To use a direct method the optimal control problem must be discretised and transformed into a non-linear programming problem. This was done in Matlab and solved with the function *fmincon* [43] included in the Optimization Toolbox. Specifically the method used was direct single shooting.

The control was parametrised as piece-wise constant with  $u_1, u_2, \dots, u_{3N+1}$  over time intervals  $T = [t_0, t_1, \dots, t_N]$ . An NLP state vector was introduced as

$p = [f_{x1}, f_{y1}, f_{z1}, \dots, f_{xN}, f_{yN}, f_{zN}, dt]$  which then contains all optimisation variables. Here  $f_{ij}$  is a nondimensional thrust component at step  $j$ , and  $dt$  is the size of the nondimensional time step. The dynamics were discretised by propagating the state with numerical integration of equations (3.14) by use of *ODE45* creating a state matrix dependent on the optimisation variables. From this the non-linear constraints could then be defined.

The equality constraints  $c_{eq} = 0$  were that the final position coordinates must coincide with the sub-Lagrange point  $[x_N - x_{final}, y_N, z_N]$  and final velocities must be small  $[v_{x,N} - v_{tol}, v_{y,N} - v_{tol}, v_{z,N} - v_{tol}]$ .

For inequality constraints  $c \leq 0$  then maximal thrust was defined for all time intervals  $f_i^2 - f_{max}^2$  ( $\vec{f}_i = [f_x, f_y, f_z]$ ,  $i = 1, \dots, N$ ) and since the mass was continually decreasing then a mass constraint was only imposed at the final point  $m_{dry} - m_f$ .

Two different cost functions were used, minimal time and minimal fuel. With every time step at the same size the total elapsed time is  $N \cdot dt$ , thus the minimal time cost function was defined as  $cost = dt$ . Minimal use of fuel is equivalent to maximal final mass and the cost function in this case was  $cost = -m_f$  (which is to be minimised).

In the implementation the number of intervals in which the control is constant was chosen as  $N = 20$ , and for each of these intervals the dynamics were propagated for  $N_{sim} = 100$  number of steps. The tolerance for final velocity was set to  $v_{tol} = 10^{-4} = 3$  m/s as was done in [6].

## 3.5 Results

### 3.5.1 Choice of ion thruster

Electric thrusters with a higher specific impulse require less propellant to execute maneuvers, which reduces cost both directly from the propellant and indirectly by less mass needing to be launched to low-Earth orbit. However these thrusters often consume more power and the spacecraft must then be equipped with more solar panels, which instead increases the launch mass. Therefore it was decided to run simulations comparing different thrusters to see how much the parameters would change the amount of mass and propellant required for an escape trajectory.

From Table 2.1, the solar panels were assumed to have a power output of 165 W/kg

and the mass contribution from this to achieve the required amount of power for each thruster was calculated. In order to cover the times when solar power is not available, such as when the spacecraft is in eclipse, batteries with an equivalent specific power [44] of the solar panels are also equipped. The payload mass was for now be set to 100 kg and includes systems such as computer, sensors and trackers since the sunshade satellites will need these once in place for station-keeping. The dry mass used in the simulations is then comprised of payload mass, thruster and IP-specific subsystems, and the solar cells with batteries. These values can be found in Table 3.2.

Table 3.2: Mass distribution and total dry mass for different thrusters types. Thruster weight includes the mass of required subsystems. These values are approximations.

Dry mass for different thrusters				
Thruster	Weight	Power	Power system weight	Dry mass
NEXT	58 kg [45]	6.8 kW	82 kg	240 kg
BPT-4000	32 kg <sup>1</sup> [46]	4.5 kW	55 kg	187 kg
AEPS	99 kg [47]	13.5 kW	164 kg	363 kg

The resulting trajectories are displayed in Figure 3.3 and values in Table 3.3.

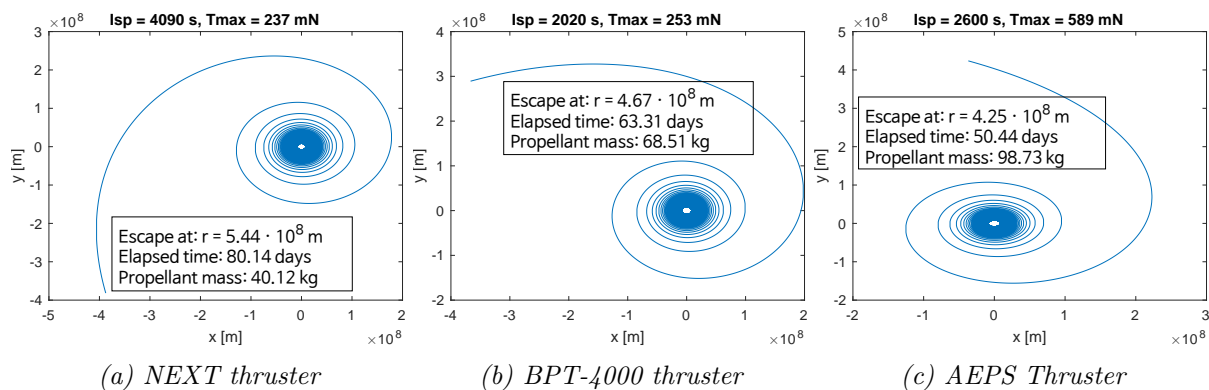


Figure 3.3: Plots of escape from Earth from a low Earth orbit, with an initial altitude of 2000 km, for different thrusters.

Table 3.3: Simulation results for launch from LEO to escape with respective dry mass and specific impulse.

Simulation for different thrusters					
Thruster	$I_{sp}$	Initial mass	Propellant mass	$m_{prop}/m_0$	$t_{escape}$
NEXT	$\sim 4090$ s	280.9 kg	40.12 kg	14.3 %	80.14 days
BPT-4000	$\sim 2020$ s	257.2 kg	68.51 kg	26.6 %	63.31 days
AEPS	$\sim 2600$ s	463.6 kg	98.73 kg	21.3 %	50.44 days

In order to weigh the results of thruster performance against power demands an estimated cost could be beneficial. Different kinds of propellants were discussed in section 2.2.5 and

<sup>1</sup>Exact weights for subsystems other than PPU could not be found, instead similar values were assumed as in [45]

all the selected thrusters run on Xenon, the cost of which was assumed to be 1800 \$US/kg. The same Launch-to-LEO cost as in reference [5] was used, this being a low prospective estimate of 50 \$US/kg.

Table 3.4: Distribution of cost for escape trajectories with a payload of 100 kg.

Estimated cost					
Thruster	Propellant mass	Propellant cost	Launch mass	Launch-to-LEO cost	Total cost
NEXT	40.12 kg	72 216 \$US	280.9 kg	14 045 \$US	86 261 \$US
BPT-4000	68.51 kg	123 318 \$US	257.2 kg	12 860 \$US	136 178 \$US
AEPS	98.73 kg	177 714 \$US	462.7 kg	23 135 \$US	200 849 \$US

The lowest total cost option as seen in Table 3.4 is then the NEXT thruster, exhibiting a balance between low structural mass and efficient use of propellant. However it was the trajectory which took the longest amount of time, at around 80 days compared to 63 and 50 days for the BPT-4000 and AEPS respectively. This is most likely due to a combination of its lower maximal thrust magnitude coupled with its moderate dry mass as compared to the other two thruster, outweighing the higher specific impulse. Since the mission of placing the sunshade system is not time critical this was not regarded as a significant issue.

### 3.5.2 Escape time for different initial parking orbits

The numerical results for different launch parking orbits are presented in Table 3.5. For all altitudes thrust and  $I_{sp}$  value provided by the NEXT Thruster is used (see Table 2.2).

Table 3.5: Numerical results for propellant mass using  $T_{max} = 237$  mN.

Different altitude for initial parking orbits using NEXT thruster				
Altitude in LEO	Analytical initial mass	Propellant mass	$m_{prop}/m_0$	$t_{escape}$
600 km	240 + 49.7 kg	45.4 kg	15.7 %	91 days
1400 km	240 + 46.8 kg	42.5 kg	14.8 %	85 days
2000 km	240 + 44.9 kg	40.7 kg	14.3 %	82 days

There is a certain discrepancy between the analytical calculations and numerical results for propellant mass required during the escape trajectory. In the analytical case semi-major axis tends to infinity for the calculation of required delta-V. Although for numerical computation then infinity is not practicable, and it is more suitable to use the specific orbital energy as a stopping condition instead. As a consequence, it is expected that the numerically determined propellant mass is less than the analytical results since the semi-major axis has a finite value at escape. Numerical and analytical results converge, specifically for the altitude of 2000 km, when instead of using infinity  $a_f$  is substituted with the escape radius for the NEXT Thruster. The resulting delta-V reduces to 6.040 km/s, leading to same propellant mass as the one which was numerically attained.

As electric propulsion is a fairly fast propulsion method, lower parking orbits do not

increase escape time considerably. As stated previously, low parking orbits may be beneficial in terms of minimising total number of launches. This warrants further research in terms of payload gains, however going forward in this thesis an altitude of 2000 km is used in order to best compare electric propulsion with solar sailing as in [6].

### 3.5.3 Escape trajectory for sunshade system

With the NEXT thruster the simulation of escape trajectories was carried out for the two sunshade compositions which were outlined in [5]. This was detailed in section 2.1.3, and in short the different values of the optical property  $Q$  for the sunshade gave the required areal densities  $\rho_A = 21.9 \text{ g/m}^2$  for  $Q = 0.5$  and  $\rho_A = 8.8 \text{ g/m}^2$  for  $Q = 0.2$ . With a bus mass  $m_{bus}$  comprised of 140 kg for the thruster and 44 kg for solar shade subsystems, as well as a sail density of  $\rho_{sail} = 4 \text{ g/m}^2$ , the necessary sail area  $A_{sail}$  and resulting sailcraft mass  $m_{dry}$  was determined according to

$$m_{dry} = \rho_{sail} \cdot A_{sail} + m_{bus} = \rho_A \cdot A_{sail} \implies A_{sail} = \frac{m_{bus}}{\rho_A - \rho_{sail}} \quad (3.18)$$

The resulting sail areas and dry masses of the sailcraft are displayed in Table 3.6.

Table 3.6: Individual shade area and spacecraft dry mass for the optical parameters  $Q$ .

Sail area and dry mass			
$Q$	$\rho_A$	$A_{sail}$	$m_{dry}$
0.5	21.9 g/m <sup>2</sup>	10 279 m <sup>2</sup>	225.1 kg
0.2	8.8 g/m <sup>2</sup>	38 333 m <sup>2</sup>	337.3 kg

The simulation was then carried out from LEO at a 2000 km altitude until full escape from Earth and yielded the trajectories in Figure 3.4 and specific values are presented in Table 3.7.

Table 3.7: Values obtained from simulation of escape for  $Q$ -values.

Escape simulation for the two $Q$ -values				
$Q$	Dry mass	Propellant mass	Final radial distance	$t_{escape}$
0.5	225.1 kg	38.3 kg	$5.264 \cdot 10^8 \text{ m}$	75.04 days
0.2	337.3 kg	57.9 kg	$6.439 \cdot 10^8 \text{ m}$	113.47 days

Compared to solar sailing, the mass of each sailcraft has increased from 55 kg to 264 kg (an increase of 380 %) or from 81 kg to 396 kg (an increase of 389 %) depending on which  $Q$ -value is used.

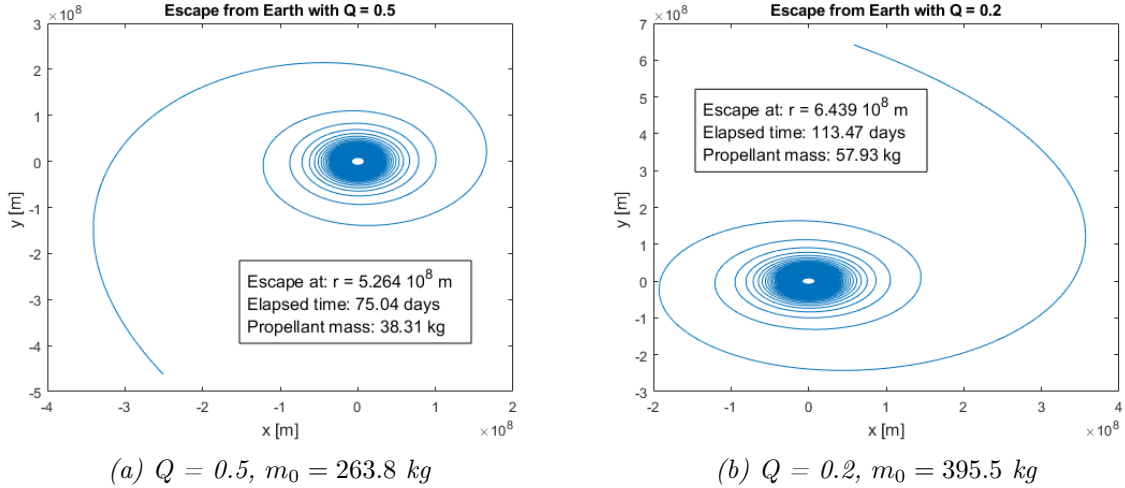


Figure 3.4: Plots for launch from LEO to escape with the mass of the sunshade for each  $Q$ -value included in the dry mass.

In order to produce the collective area of  $3.79 \cdot 10^{12} \text{ m}^2$  the number of sailcrafts  $N$  was computed and also the grand total mass  $M$  of the sunshade configuration as a whole. This was then compared to the values  $N_s, M_s$  obtained by using solar sailing as means of propulsion. Note that the total mass includes propellant mass in the case of electric propulsion, which is to be consumed by the time the satellites are in place (and thus total final mass is equal for both propulsion methods).

Table 3.8: The total number of spacecrafts  $N$ , their combined wet mass  $M$  and propellant mass  $M_{prop}$  along with the corresponding values  $N_s, M_s$  for solar sailing.

Number of sailcrafts and mass					
$Q$	$N = \frac{A_{tot}}{A_{sail}}$	$M$	$M_{prop}$	$N_s$	$M_s$
0.5	$3.7 \cdot 10^8$	$9.7 \cdot 10^{10} \text{ kg}$	$1.4 \cdot 10^{10} \text{ kg}$	$1.5 \cdot 10^9$	$8.3 \cdot 10^{10} \text{ kg}$
0.2	$9.9 \cdot 10^7$	$3.9 \cdot 10^{10} \text{ kg}$	$5.7 \cdot 10^9 \text{ kg}$	$4.2 \cdot 10^8$	$3.4 \cdot 10^{10} \text{ kg}$

As evident by Table 3.8, the total launch mass for the project would increase by 15-17 % which equates to an estimated additional cost of 300-700 billion US\$ (for propellant). There is also a significant reduction in time required for the maneuver, with 75 days compared to 531 days ( $Q = 0.5$ ) and 113 days compared to 285 days ( $Q = 0.2$ ) respectively.

### 3.5.4 Travel to the sub-Lagrange point

Since the satellites now carry the additional weight of the electric thrusters the area of each individual sail has increased to compensate. This might affect the viability of using solar sailing as the means of propulsion from the point of escape to the final sub-Lagrange point. An alternative is then to use the ion thrusters to carry the sunshades the entire way, and can be done either to minimise the time required for this final maneuver or the amount of additional propellant. Both results have been included in this section.

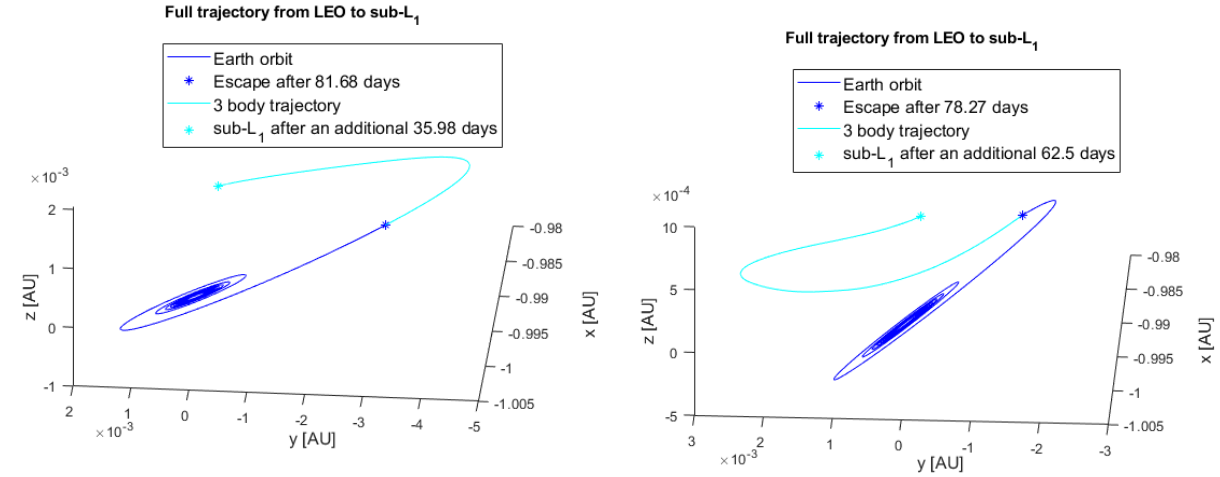
The final point is located on the Sun-Earth line with  $L'_1 = 0.0158 \text{ AU}$  from the Earth,

corresponding to the coordinates  $[x, y, z] = [-(1 - \mu) - L'_1], 0, 0] \approx [-0.984197, 0, 0]$ . In order to cover both the escape spiral and the trajectory to  $L'_1$  additional propellant was added while using the same dry mass as specified in Table 3.6. The escape from Earth was re-computed in the same way and with the same thruster parameters and initial orbit in LEO as before. These resulting values were subsequently transformed into the non-dimensional synodic coordinate system as described in 3.2.3 and a trajectory to  $L'_1$  determined using the direct method implemented as in 3.4.2.

With a low  $Q$  side of  $Q = 0.5$ , the coordinate transformation is presented in Table 3.9, trajectories in Figure 3.5, velocities in Figure 3.6 and thrust in Figure 3.7.

Table 3.9: Values for change of coordinates from Earth-Centered inertial to non-dimensional synodic with  $Q = 0.5$  for both cases of minimal time and minimal propellant.

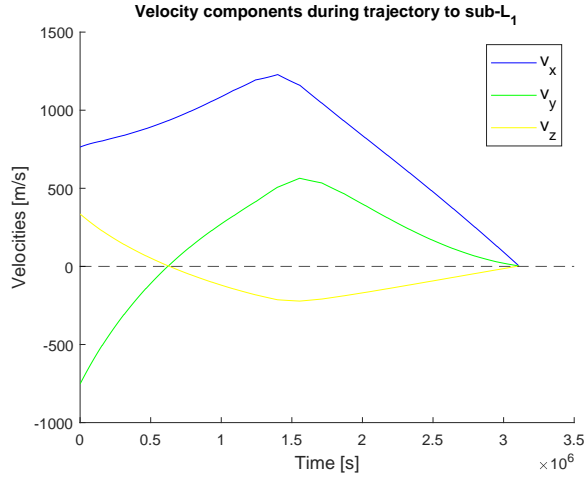
Coordinate system transformation $Q = 0.5$						
System, minimal	x	y	z	$v_x$	$v_y$	$v_z$
ECI, time	$-1.1484 \cdot 10^8$ m	$-5.3641 \cdot 10^7$ m	0 m	862.6 m/s	-842.1 m/s	0 m/s
CR3BP, time	-1.0008	-0.0033	0.0014	0.0257	-0.0252	0.0112
ECI, prop	$4.6564 \cdot 10^8$ m	$-2.6810 \cdot 10^8$ m	0 m	1077.1 m/s	568.9 m/s	0 m/s
CR3BP, prop	-0.9969	-0.0016	0.0007	0.0345	0.0144	-0.0076



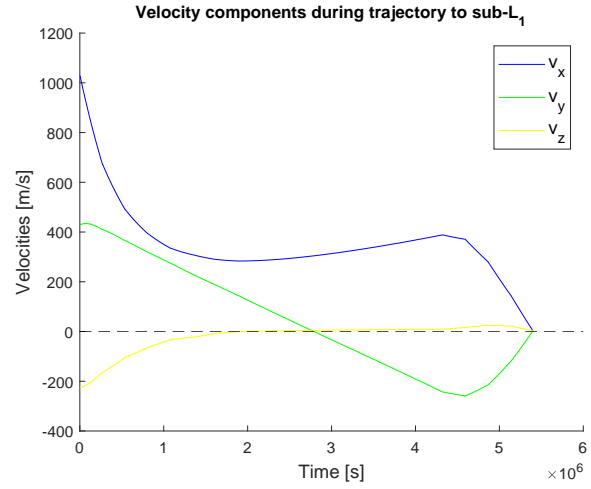
(a) Minimal time,  $m_{prop} = 18.36$  kg,  $m_{0,0} = 286.60$  kg,  $m_{0,esc} = 244.90$  kg

(b) Minimal propellant,  $m_{prop} = 6.02$  kg,  $m_{0,0} = 274.90$  kg,  $m_{0,esc} = 234.94$  kg

Figure 3.5: Trajectories to  $L'_1$  for minimal time and minimal propellant with  $Q = 0.5$ . The initial mass at the start in Earth orbit is  $m_{0,0}$  while  $m_{0,esc}$  is the mass at the point of escape from Earth, and  $m_{prop}$  only denotes propellant for the 3 body trajectory.

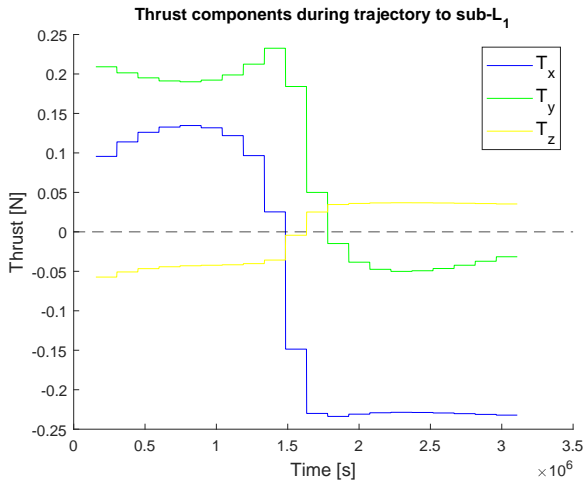


(a) Minimal time

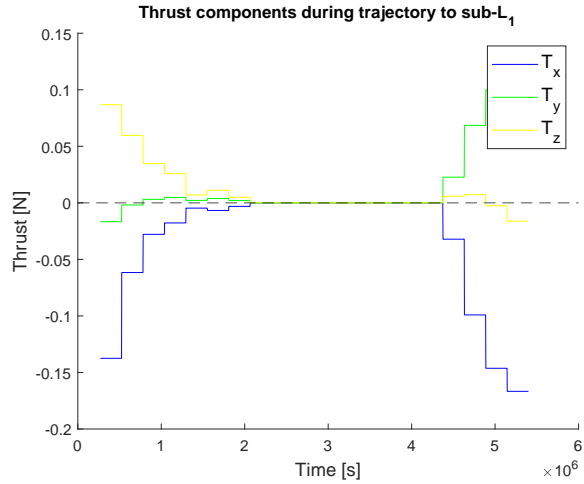


(b) Minimal propellant

Figure 3.6: Velocity components during transfer to  $L'_1$  for  $Q = 0.5$



(a) Minimal time



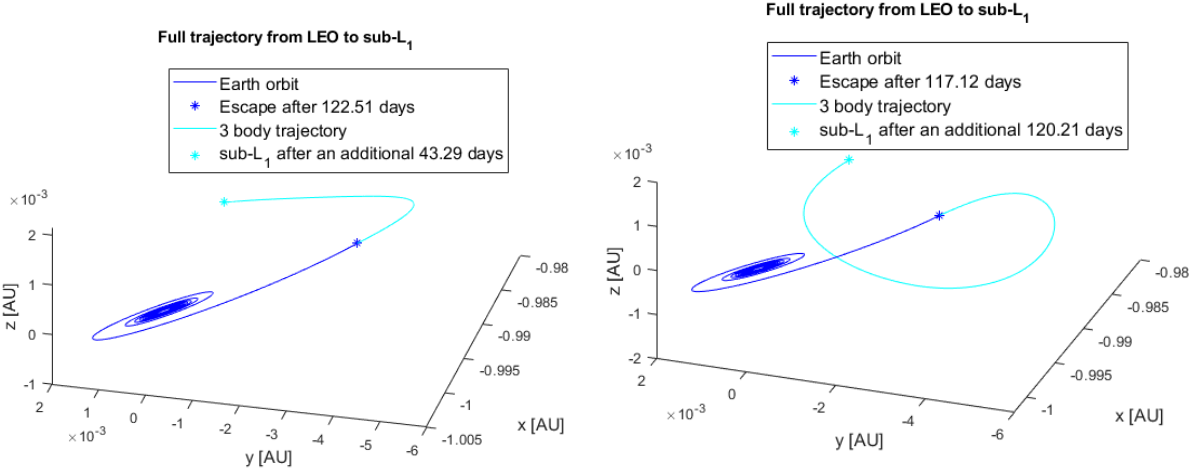
(b) Minimal propellant

Figure 3.7: Piece-wise constant thrust throughout the trajectory for  $Q = 0.5$

With a low  $Q$  side of  $Q = 0.2$ , the coordinate transformation is presented in Table 3.10, trajectories in Figure 3.8, velocities in Figure 3.9 and thrust in Figure 3.10.

Table 3.10: Values for change of coordinates from Earth-Centered inertial to non-dimensional synodic with  $Q = 0.2$  for both cases of minimal time and minimal propellant.

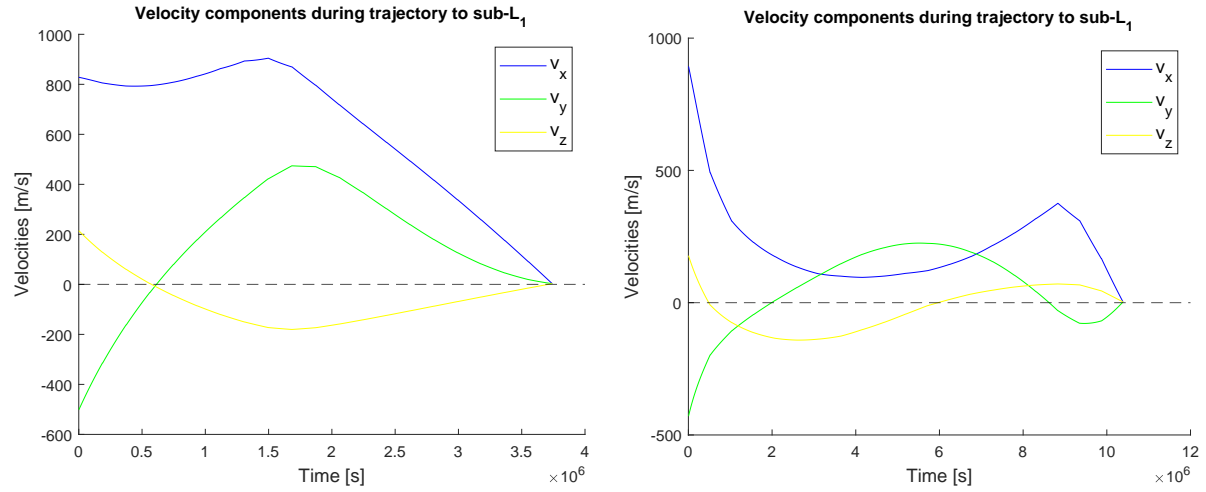
Coordinate system transformation $Q = 0.2$						
System, minimal	x	y	z	$v_x$	$v_y$	$v_z$
ECI, time	$3.1421 \cdot 10^7$ m	$-6.6780 \cdot 10^8$ m	0 m	950.0 m/s	-538.4 m/s	0 m/s
CR3BP, time	-0.9998	-0.0041	0.0018	0.0278	-0.0168	0.0072
ECI, prop	$9.6378 \cdot 10^7$ m	$-6.4687 \cdot 10^8$ m	0 m	1010.0 m/s	-444.8 m/s	0 m/s
CR3BP, prop	-0.9994	-0.0040	0.0017	0.0300	-0.0144	0.0059



(a) Minimal time,  $m_{prop} = 22.09$  kg,  $m_{0,0} = 426.40$  kg,  $m_{0,esc} = 363.86$  kg

(b) Minimal propellant,  $m_{prop} = 9.98$  kg,  $m_{0,0} = 408.00$  kg,  $m_{0,esc} = 348.20$  kg

Figure 3.8: Trajectories to  $L'_1$  for minimal time and minimal propellant with  $Q = 0.2$ . The initial mass at the start in Earth orbit is  $m_{0,0}$  while  $m_{0,esc}$  is the mass at the point of escape from Earth, and  $m_{prop}$  refers only to the propellant consumed during the 3 body trajectory.



(a) Minimal time

(b) Minimal propellant

Figure 3.9: Velocity components during transfer to  $L'_1$  for  $Q = 0.2$

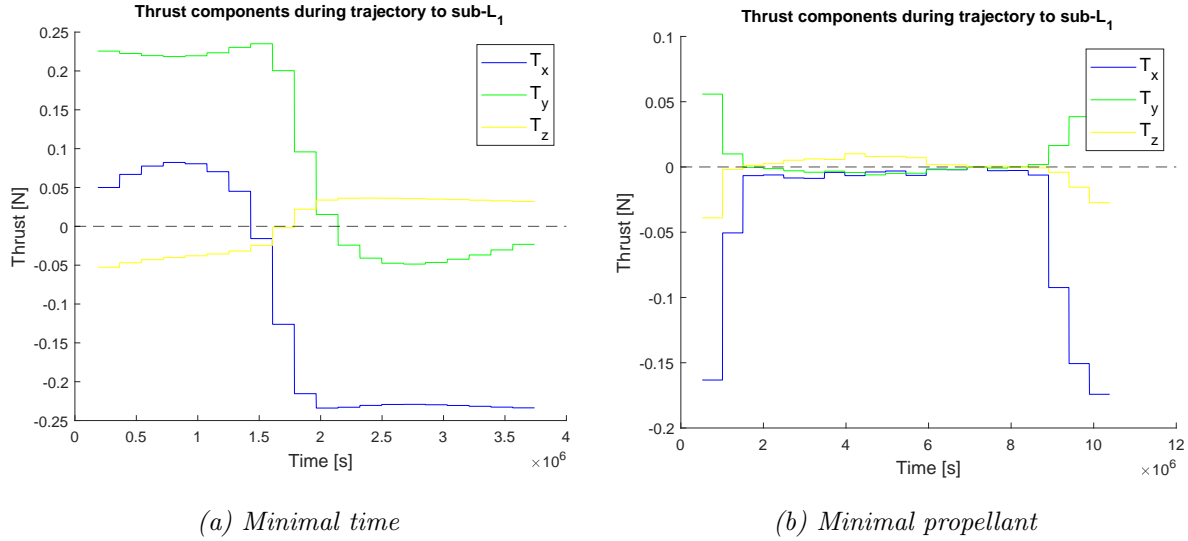


Figure 3.10: Piece-wise constant thrust throughout the trajectory for  $Q = 0.2$

A summary of results for the full trajectory with both values  $Q$  can be found in Table 3.11 below.

Table 3.11: Results for the trajectories to the sub-Lagrange point. Total mass is the mass of all the satellites with propellant combined, propellant mass refers to total amount of propellant consumed for the full trajectory, and transfer time is measured from start in LEO to arrival at  $L'_1$ .

Summary of results for transfer to sub- $L_1$					
$Q$	Minimal	Initial mass	Total mass	Propellant mass	Transfer time
0.5	Time	286.6 kg	$10.6 \cdot 10^{10}$ kg	$2.2 \cdot 10^{10}$ kg	117.66 days
0.5	Propellant	274.9 kg	$10.2 \cdot 10^{10}$ kg	$1.7 \cdot 10^{10}$ kg	147.77 days
0.2	Time	426.4 kg	$4.2 \cdot 10^{10}$ kg	$8.4 \cdot 10^9$ kg	165.80 days
0.2	Propellant	408.0 kg	$4.0 \cdot 10^{10}$ kg	$6.9 \cdot 10^9$ kg	237.33 days

Assuming that a suitable trajectory would be a combination of minimal time and minimal propellant, and once again comparing the launch mass using Table 3.8, the mass increase is on average 25 % for  $Q = 0.5$  and 21 % for  $Q = 0.2$ . This corresponds to  $\sim 10^{10}$  kg of propellant and could be equated to a launch cost of 350-1100 billion US\$ for propellant mass alone.

With solar sailing the entire trajectory had a travel time of 603 days ( $Q = 0.5$ ) or 373 days ( $Q = 0.2$ ). Even in the minimal propellant cases the electric thrusters permitted much shorter transfer times, with an estimated time 24.5 % that of solar sailing with  $Q = 0.5$  and 63.6 % with  $Q = 0.2$ . The corresponding values for minimal time are 19.5 % and 44.5 %.

# Chapter 4

## Discussion and Conclusions

### 4.1 Discussion

#### 4.1.1 Partial and full trajectory with ion propulsion

The most critical segment of the trajectory for each sunshade is the escape from Earth. This is because of the Van Allen radiation belts, starting at around a 600 km altitude and extending to 60 000 km, as well as space debris and the complicated attitude control required during such a transfer. Additionally, the remaining trajectory can be completed using electric thrusters as well, eliminating the need for the shades to function as solar sails. Parameters for the thruster affects the mass and time required for the manoeuvre, and one with a high specific impulse but moderate power requirements was selected as suitable in order to limit overall costs.

The partial trajectory, meaning where electric thrusters were only used to escape Earth, increased the launch mass of the sunshade system by 15 - 17 % equating to propellant mass in the order  $10^9 - 10^{10}$  kg. If electric thrusters were instead used for the full trajectory, where the sunshades would not need to act as means of propulsion, the increase of the system's mass was around 21 - 25 % of that obtained with solar sailing and this case gave a required propellant mass of  $\sim 10^{10}$  kg. In both cases this equates to increased launch costs in the order 300-1000 billion US\$ and further costs due to the propellant itself, meaning that electric thrusters is a more expensive alternative for the sunshade project than solar sailing would be. Even so, depending on future development of solar sailing as a means of propulsion, it might be the more feasible option.

Another important result is that in all the cases studied electric propulsion permitted much shorter transfer times than solar sailing did. For the best case with minimal time, the full trajectory took approximately 20 % of the time, and on average the ratio was circa 22 % and 54 % for  $Q = 0.5$  and  $Q = 0.2$  respectively. This aspect is especially advantageous considering that in the original study optimal orientation of the sail was assumed at all times, and thus the real sailing transfer time could be much longer. While not a pivotal aspect of the project, a shorter transfer time is beneficial because of the lessened radiation exposure of the electrical equipment, solar panels and of course the shade membranes themselves. However, this study has not included the diminished performance of the thrusters and solar panels due to the degradation which does take place,

and as a consequence the real transit times could be larger than the ones presented in this study as well.

#### 4.1.2 Initial parking orbits and number of launches

In section 3.3.1 and 3.5.2 different initial parking orbits in LEO were studied, meaning the different altitudes from which ion thrusters would commence the escape spiral transfer. The difference between starting at 600 km to 2000 km was 5 kg of more propellant and 9 days of travel time for the lower altitude, two comparably quite small additions to the manoeuvre as a whole. However, the low initial orbit would introduce energy losses due to atmospheric drag which in turn would also give rise to additional wear and reduced lifetime of electrical components, as well as possible complications due to low orbiting satellites such as the Starlink constellation. Nonetheless, the reason a lower altitude should be considered are the possible payload gains.

An analysis of launching vehicles was performed by [6] and found that the most cost-effective option in development was the Starship rocket by SpaceX. The Starship is to be a fully reusable a two stage rocket, and has a payload capacity of 100 000 kg when launched to a 500 km high-inclination orbit. However this would be reduced to one-fifth if the final orbit was 40 000 km [48, p.6]. This would mean that the total number of launches could be significantly reduced if a low initial parking orbit was used instead of the higher one required for solar sailing. Starting at a low orbit - especially below 1000 km - is not feasible for solar sailing, primarily because of the much larger impact of atmospheric drag on the sails but also the risk space debris poses to their integrity. In this regard, electric propulsion would be advantageous since the addition of required propellant mass and time is minor.

#### 4.1.3 Chemical propulsion to geostationary orbit

The large mass of the sunshade project that must be launched as well as the long distance that must be covered for the final position makes chemical propulsion somewhat ineffective for the whole space mission. However chemical propulsion is a well-tested propulsion method and it provides benefits in terms of performing rapid orbital maneuvers or shielding the sunshades from radiation related damages as well as space debris.

Thus another possible propulsion scheme for the sunshade configuration is to use chemical propulsion well into geostationary transfer orbit (GTO) and thereafter begin solar sailing as means of propulsion. This allows sunshades to spend less time in the Van Allen radiation belts which reduced the negative effects on the bus components for the sunshades. However, increasing the target orbit from LEO to GTO increases the total number of launches as the payload capacity of the Starship decreases from maximum of 150 000 kg in LEO to 21 000 kg in GTO [48, p.6]. The significant reduction of payload capacity results in five fold rise of total number of launches and consequently the total cost of the Sunshade project.

#### 4.1.4 Environmental impact and production

The Starship propellant is comprised of methane as fuel and liquid oxygen as oxidizer. The exhaust from the fuel can be decreased to almost zero, provided that the propulsion unit is efficient and combustion is complete [49]. Methane provides great environmental benefits compared to other chemical propellants such as kerosene and hydrogen, as it burns more cleanly than kerosene and provides more energy than hydrogen. On the other hand, most methane today comes from fossil fuel extraction and during production a significant amount can escape into the atmosphere. As methane is a potent greenhouse gas this leaked gas accelerates global warming [50]. There have been suggestions ([51], [52]) to produce more "green" methane through a variety of methods although more research is required. Obtaining the large amount of methane needed for the sunshade project will then contribute to the global wide-scale mining of fossil fuels, counterproductive to the aim of the project.

Xenon is a noble gas and is mainly contained to the Earth's atmosphere, although small amounts can be found in the seas as well as in the Earth's crust. Worldwide production of xenon is less than 1 tonne per year but reserves of the gas amounts to 2 billion tonnes [53, p.8]. For the electrically propelled sunshade project the total propellant mass of xenon required is of the order  $10^{10}$  kg. This amounts to a staggering 1 % of all xenon reserves found on Earth. This level of xenon production would consume a huge amount of energy as it is extracted from the atmosphere, and a complete change in the current approach since most xenon production today is a byproduct of other air liquefaction processes. According to reference [54], a direct xenon extraction plant with 100 % extraction efficiency might be able to produce 1 tonne of xenon per year with same cost per kilogram as used in section 3.5.1. For the electrical sunshade project, up to a million of comparable xenon extraction plants must be built beforehand. To put this into perspective, approximately 4 000 air separation plants have been built by the lead supplier since 1902 [55]. Furthermore, the extraction plants must be able to function simultaneously during a 20-year period requiring a huge amount of electricity. These preparations may drastically increase the cost for electrically propelled sunshade project.

Xenon is preferred with ion engines and Hall thrusters, however issues of cost and availability make argon and krypton, also noble gases, potential substitutes. Performance specifications are diminished with argon and krypton, since these atoms are less massive than xenon and require more energy to ionize. A related downside of using krypton or argon is the increase in the trajectory time. With an  $I_{sp}$  of 2000 s, a krypton mission takes 16 % longer than a xenon mission while an argon mission requires 63 % more time. For larger specific impulses such as NEXT Thruster, these delays get shorter [54]. A comprehensive study between krypton and argon for the choice of propellant has been conducted in [54] and the most promising propellant after xenon, in terms of noble gases, is krypton. As krypton can be produced similarly to xenon but there is roughly 10 times more of it in the atmosphere, a krypton mission will have a cost about  $\frac{1}{10}$  that of xenon.

Although xenon is a noble gas, it is nonetheless more reactive than other noble gases. Emitting large amount of ionized xenon in the exosphere during an escape trajectory will change its composition, as xenon is naturally absent at such altitudes [53]. Furthermore,

as the use of electric propulsion at such great scale has never been attempted before, it is unclear what impact a large amount of ions in the exosphere will have on the atmospheric chemistry. Xenon has shown to have some potential for chemical reactions in the lower altitudes [53, p.25-27], and the choice of propellant makes this type of analysis compulsory for other non-inert propellants, e.g. iodine.

#### 4.1.5 Solar sail area and feasibility

Equipping the satellites with electric thrusters would raise the dry mass of the spacecrafts considerably, and using estimates based off of power requirements this increase was found to be close to 400 %. In order for the minimal mass point along the Sun-Earth line to be at equilibrium, then the area of each individual sail would need to increase in order to off-set the gravitational forces. This area was computed by using the areal densities for each sail efficiency factor and the results are displayed in Table 3.8. The resulting sail areas are very large, meaning that the additional mass might affect the feasibility of using solar sailing to travel to the sub-Lagrange point. If  $Q$  was equal to 0.5 the sail area was  $\sim 10\,000\text{ m}^2$ , whereas  $Q = 0.2$  gave a sail area nearly four times that. The size of the solar sail affects the viability of it to be used as a means of propulsion, and much research is ongoing within the field. For example, the Solar cruiser mission is set to launch in 2025 and its aim is to demonstrate solar sail technologies by traveling to the vicinity of  $L_1$ . This mission features a sail membrane developed by NASA with an area of  $1653\text{ m}^2$ , but is however scalable - even to sails larger than  $10\,000\text{ m}^2$  [56].

Using the sail efficiency factor which is state-of-the-art currently, then the resulting sail feasibly be used as a means of propulsion, assuming that prerequisite development would take place before implementation of the project. On the other hand, the low, prospective value of  $Q = 0.2$  gave an area which could most likely not be used for sailing. The alternatives in that case are then to either select a sub-Lagrange point which does not coincide with the minimal mass point for the system or to use electric thrusters for the entire trajectory. The latter option might warrant further study to determine if an area this large could even have enough maneuverability for station-keeping.

#### 4.1.6 Accuracy and assumptions

##### Numerical results and parameters

Rather than extrapolating and estimating future development in electric thruster technology, specific designs with known specifications were studied. The main reason for this was so that their tabulated power requirements could be used in order to find approximate ranges for the spacecrafts dry mass. By the time of implementation of the sunshade project many of the technologies involved are likely to have progressed much further and the spacecraft parameters could be quite different.

The solutions for trajectories to  $L_1$  have been computed in a chaotic system, meaning that very different outcomes can be obtained even if the variations in initial conditions are small. In particular parameters such as allotted propellant mass affected the coordinates and velocities at the point of escape, and thus simulations yielded dissimilar values for elapsed time and consumed propellant after only a small change of the initial mass.

Furthermore, the direct method does not necessarily converge to a globally optimal solution when the trajectory is computed. This means that the resulting trajectories, the values for time, and for required mass are only estimates suitable for rough comparisons.

Transformations between the celestial coordinate systems depend on the time of year, as the  $x$ -axis of the ECI coordinate system is fixed relative to the stars while  $x$ -axis of the CRTBP follows the rotation of the Earth around the Sun, and is always aligned with the Sun-Earth line. These coincide during the vernal equinox, and since the date for the launch of each satellite of the constellation will differ the axes were assumed to be parallel at the time of escape.

The first trajectory segment, the escape from Earth, assumed planar dynamics. This model works adequately when only gravitational and centripetal forces affect the spacecraft. If perturbation forces, such as Earth oblateness effects, were included in the computations these could contribute to a  $z$ -displacement, and while this should not majorly affect the results it is worth noting. More accurate trajectories could be determined by using more refined methods and many simulation programs for similar purposes have already been developed, for example software such as the General Mission Analysis Tool (GMAT) by NASA.

### **Solar electric propulsion and Earth's shadow**

Both solar sailing and solar electric propulsion (SEP) are propulsion methods that use sunlight to create thrust. This subjects certain requirements on the design of the spacecraft. For solar sailing, the results are based on an optimal control system that optimises the orientation of the solar sail such that the maximal thrust possible for that thrust segment can be achieved. For SEP the maximal thrust occurs only when solar panels are directed towards the Sun providing the power-consuming thrusters with maximum electric power, requiring a control system which was assumed to be equipped by the spacecrafts. To be able to thrust during eclipses, additional mass in terms of rechargeable batteries has been accounted for in section 3.5.1. This is a common practice for time driven space missions as it allows for shorter transit time and less time spent in radiation belts. However, thrust through eclipses restricts the maximal thrust available at the sunlit portion of the trajectory as some of the solar power collected at this time must be used to recharge the batteries, and the extent of the decrease in maximal thrust merits further study.

Meanwhile, the sunshade project is not a time critical mission and cost-wise along with feasibility of solar sails it may be more advantageous to let spacecraft coast during eclipses. This will reduce the power output mass by half, replacing it with a longer transit time and as a result higher degradation of solar cells and thrusters due to radiation. Consequently, the dry mass of a single satellite may still increase in order to incorporate more radiation shielding equipment, the mass of propellant tanks, or other mass margins due to preliminary design [57]. Therefore, the dry mass of the propulsion systems in this thesis are only approximate. For more accurate values, weighing of the trade-offs between mass of batteries and radiation related damages to the subsystems must be done.

## 4.2 Summary and Conclusions

In order to limit the effects of global warming and reduce the temperature increase by 1 °C, a space-based geoengineering scheme was proposed which would block 1 % of incident solar radiation. This solution could be implemented in parallel to other environmental efforts. The scheme would consist of the deployment of a large number of sunshades in the vicinity of the first Lagrange point of the Sun-Earth system, and these would constitute a sunshade system which would shield Earth from the solar radiation. As an extension of a feasibility study for the implementation of this large-scale mission, the focus was on comparing electric propulsion to solar sailing as a means of propulsion for the spacecrafts. Firstly the background covered essentials in electric propulsion systems and spaceflight mechanics, and then an investigation was performed by defining the spacecraft configurations and computing trajectories to a point of escape from Earth as well as the final equilibrium point. In order to account for the power demands of electric thrusters each spacecraft's dry mass would need to become approximately 5 times larger compared to the solar sailing configuration, and for the full mission the combined mass of the required propellant mass was of the order  $10^{10}$  kg. The additional launch cost due to higher wet mass of 15 - 25 % was estimated to the order of 300-1000 billion US\$. Despite the higher associated costs, electric propulsion could still be a beneficial choice for the implementation of a sunshade system since it would allow shorter transfer times from Earth for each shade. It was found that the transfer time with electric propulsion would be about one-half or one-fifth that of solar sailing, depending on what spacecraft parameters are deemed feasible. A shorter transfer time is preferable because it reduces the radiation exposure and subsequent degradation of the spacecraft's systems, most notably the shade membranes themselves. Another advantage of electric propulsion over solar sailing is that it allows a much lower initial parking orbit, and while this would increase the aforementioned radiation exposure it would also reduce the launch costs since a lower altitude entails a higher payload capacity for most launchers. Nevertheless, the use of electric propulsion at this scale requires many prior advancements in inert propellant extraction and possibly also a wide-scale construction of propellant manufacturing plants.

# References

- [1] R. Lindsey and L. Dahlman, “Climate change: Global temperature,” *Climate.gov*, vol. 16, 2020, accessed 20 April 2022. [Online]. Available: <https://www.climate.gov/news-features/understanding-climate/climate-change-global-temperature>
- [2] A. Buis, “A degree of concern: Why global temperatures matter,” *NASA’s Global Climate Change Website*, vol. 16, 2020, accessed 20 April 2022. [Online]. Available: <https://climate.nasa.gov/news/2865/a-degree-of-concern-why-global-temperatures-matter/>
- [3] “The paris agreement,” accessed 20 April 2022. [Online]. Available: <https://unfccc.int/process-and-meetings/the-paris-agreement/the-paris-agreement>
- [4] C. R. McInnes, “Space-based geoengineering: challenges and requirements,” *Proceedings of the Institution of Mechanical Engineers, Part C: Journal of Mechanical Engineering Science*, vol. 224, no. 3, pp. 571–580, 2010.
- [5] C. Fuglesang and M. G. de Herreros Miciano, “Realistic sunshade system at l1 for global temperature control,” *Acta Astronautica*, vol. 186, pp. 269–279, 2021.
- [6] M. García de Herreros Miciano, “Feasibility study of the implementation of a space sunshade near the first lagrangian point,” Master’s thesis, KTH Royal Institute of Technology, Stockholm, Sweden, July 2020, diva2:1464096.
- [7] J. T. Early, “Space-based solar shield to offset greenhouse effect,” *Journal of the British Interplanetary Society*, vol. 42, pp. 567–569, 1989.
- [8] R. Angel, “Feasibility of cooling the earth with a cloud of small spacecraft near the inner lagrange point (l1),” *Proceedings of the National Academy of Sciences*, vol. 103, no. 46, pp. 17 184–17 189, 2006.
- [9] B. Govindasamy and K. Caldeira, “Geoengineering earth’s radiation balance to mitigate co2-induced climate change,” *Geophysical Research Letters*, vol. 27, no. 14, pp. 2141–2144, 2000.
- [10] W. E. Wiesel, *Spaceflight dynamics*. McGraw-Hill Science, Engineering & Mathematics, 1997, vol. 1.
- [11] D. M. Goebel and I. Katz, *Fundamentals of electric propulsion: Ion and Hall thrusters*. John Wiley & Sons, 2008.

- [12] E. Choueiri and J. Ziemer, “Quasi-steady magnetoplasmadynamic thruster measured performance database,” in *34th AIAA/ASME/SAE/ASEE Joint Propulsion Conference and Exhibit*, 1998, p. 3472.
- [13] S. Mazouffre, “Electric propulsion for satellites and spacecraft: established technologies and novel approaches,” *Plasma Sources Science and Technology*, vol. 25, no. 3, p. 033002, 2016.
- [14] “Power state of the art nasa report - 3.0 power,” accessed 5 April 2022. [Online]. Available: <https://www.nasa.gov/smallsat-institute/sst-soa/power#3.1>
- [15] K. Holste, W. Gärtner, P. Köhler, P. Dietz, J. Konrad, S. Schippers, P. J. Klar, A. Müller, and P. R. Schreiner, “In search of alternative propellants for ion thrusters,” in *34th International Electric Propulsion Conference, At Kobe, Japan*, 2015.
- [16] “Deep space 1,” accessed 20 April 2022. [Online]. Available: <https://www.jpl.nasa.gov/missions/deep-space-1-ds1>
- [17] “Smart-1,” accessed 20 April 2022. [Online]. Available: [https://www.esa.int/Enabling\\_Support/Operations/SMART-1](https://www.esa.int/Enabling_Support/Operations/SMART-1)
- [18] T. Talbert, “Nasa, spacex launch dart: First planetary defense test mission,” Oct 2021, accessed 20 April 2022. [Online]. Available: <https://www.nasa.gov/planetarydefense/dart/dart-news>
- [19] J. R. Anderson, K. D. Goodfellow, J. E. Polk, V. Rawlin, and J. Sovey, “Performance characteristics of the nstar ion thruster during an on-going long duration ground test,” in *2000 IEEE Aerospace Conference. Proceedings (Cat. No. 00TH8484)*, vol. 4. IEEE, 2000, pp. 99–122.
- [20] D. A. Herman, “Nasa’s evolutionary xenon thruster (next) project qualification propellant throughput milestone: Performance, erosion, and thruster service life prediction after 450 kg,” in *57th Joint Army-Navy-NASA-Air Force (JANNAF) Propulsion Meeting*, no. E-17447, 2010.
- [21] J. Snyder, D. M. Goebel, R. R. Hofer, J. E. Polk, N. C. Wallace, and H. Simpson, “Performance evaluation of the t6 ion engine,” *Journal of Propulsion and Power*, vol. 28, no. 2, pp. 371–379, 2012.
- [22] S. Xu, B. Welander, , and R. Corey, “Testing of the ppu mk3 with the xr-5 hall effect thruster,” *35th International Electric Propulsion Conference*, p. 11, 10 2017.
- [23] R. R. Hofer, I. G. Mikellides, I. Katz, and D. M. Goebel, “Bpt-4000 hall thruster discharge chamber erosion model comparison with qualification life test data,” in *30th International Electric Propulsion Conference*, 2007, pp. 17–20.
- [24] J. Jackson, S. Miller, J. Cassady, E. Soendker, B. Welander, M. Barber, and P. Y. Peterson, “13kw advanced electric propulsion flight system development and qualification,” Aerojet Rocketdyne, Tech. Rep., 2019.

- [25] S. J. Hall, B. J. Jorns, A. D. Gallimore, H. Kamhawi, T. W. Haag, J. A. Mackey, J. H. Gilland, P. Y. Peterson, and M. Baird, “High-power performance of a 100-kw class nested hall thruster,” in *International Electric Propulsion Conference (IEPC)*, no. IEPC-2017-228, 2017.
- [26] “Our engine,” Nov 2021, accessed 20 April 2022. [Online]. Available: <https://www.adastrarocket.com/our-engine/>
- [27] H. Curtis, *Orbital mechanics for engineering students*. Butterworth-Heinemann, 2013.
- [28] N. Brisby and R. R. Rumble, “A presentation of the two-body problem,” 2002.
- [29] V. Szebehely and E. Grebenikov, “Theory of orbits-the restricted problem of three bodies.” *Soviet Astronomy*, vol. 13, p. 364, 1969.
- [30] A. Tartaglia, E. Lorenzini, D. Lucchesi, G. Pucacco, M. Ruggiero, and P. Valko, “How to use the sun–earth lagrange points for fundamental physics and navigation,” *General Relativity and Gravitation*, vol. 50, no. 1, pp. 1–21, 2018.
- [31] D. Darling, “Lagrangian points,” accessed 15 April 2022. [Online]. Available: <https://www.daviddarling.info/encyclopedia/L/Lagpoint.html>
- [32] “Lagrange points: The stunning parking lots in space,” Stargazing Mumbai, accessed 2 May 2022. [Online]. Available: <https://stargazingmumbai.in/lagrange-points-the-parking-lots-in-space/>
- [33] C. R. McInnes, *Solar sailing: technology, dynamics and mission applications*. Springer Science & Business Media, 2004.
- [34] J.-P. Sánchez and C. R. McInnes, “Optimal sunshade configurations for space-based geoengineering near the sun-earth l1 point,” *Plos one*, vol. 10, no. 8, p. e0136648, 2015.
- [35] C. Kirches, *Fast numerical methods for mixed-integer nonlinear model-predictive control*. Springer, 2011.
- [36] F. Topputo and C. Zhang, “Survey of direct transcription for low-thrust space trajectory optimization with applications,” in *Abstract and Applied Analysis*, vol. 2014. Hindawi, 2014.
- [37] N. B. LaFarge, “Autonomous guidance for multi-body orbit transfers using reinforcement learning,” 2020.
- [38] B. Daoud, “On the optimal control of the circular restricted three body problem,” 2011.
- [39] E. I. Abouelmagd, “The effect of photogravitational force and oblateness in the perturbed restricted three-body problem,” *Astrophysics and Space Science*, vol. 346, no. 1, pp. 51–69, 2013.
- [40] “Earth’s declination with respect to sun-earth-plane,” accessed 15 April 2022. [Online]. Available: <https://susdesign.com/popups/sunposition/declination.php>

- [41] “Low earth orbit,” European Space Agency, accessed 20 April 2022. [Online]. Available: [https://www.esa.int/ESA\\_Multimedia/Images/2020/03/Low\\_Earth\\_orbit](https://www.esa.int/ESA_Multimedia/Images/2020/03/Low_Earth_orbit)
- [42] H. Kawasaki, K. Konoue, H. Hoshino, Y. Kaneko, and M. Sasaki, “Interim report of super low altitude satellite operation,” in *IGARSS 2018-2018 IEEE International Geoscience and Remote Sensing Symposium*. IEEE, 2018, pp. 4066–4069.
- [43] “fmincon,” accessed 20 April 2022. [Online]. Available: <https://se.mathworks.com/help/optim/ug/fmincon.html>
- [44] “Saft battery solutions for space: Reliability and performance for over 50 years,” 2019.
- [45] M. Patterson and S. Benson, “Next ion propulsion system development status and performance,” in *43rd AIAA/ASME/SAE/ASEE Joint Propulsion Conference & Exhibit*, 2007, p. 5199.
- [46] J. Fisher, A. Wilson, D. King, S. Meyer, K. de Grys, and L. Werthman, “The development and qualification of a 4.5-kw hall thruster propulsion system for geo satellite applications—status update,” in *28th International Electric Propulsion Conference, paper-0295, Toulouse, France*, 2003.
- [47] “Aeps - advanced electric propulsion system,” Aerojet Rocketdyne, accessed 4 March 2022. [Online]. Available: <https://www.rocket.com/sites/default/files/documents/AEPS.pdf>
- [48] “*Starship User’s Guide*,” Space Exploration Technologies Corp, accessed 15 April 2022. [Online]. Available: [https://www.spacex.com/media/starship\\_users\\_guide\\_v1.pdf](https://www.spacex.com/media/starship_users_guide_v1.pdf)
- [49] T. Pultarova, “The environmental impact of rocket launches: The ‘dirty’ and the ‘green’,” accessed 15 April 2022. [Online]. Available: <https://www.space.com/rocket-launches-environmental-impact>
- [50] D. Reay, “Sources of methane - energy related,” accessed 15 April 2022. [Online]. Available: <http://www.ghgonline.org/methaneenergy.htm>
- [51] M. SHWARTZ, “Stanford scientists use microbes to make ‘clean’ methane,” accessed 15 April 2022. [Online]. Available: <https://news.stanford.edu/news/2012/july/microbes-clean-methane-072412.html>
- [52] H. Stoltz, “Emissions from spacex’s mars rocket,” accessed 15 April 2022. [Online]. Available: <https://cleantechnica.com/2019/10/30/no-you-dont-have-to-worry-about-emissions-from-spacexs-mars-rocket/>
- [53] M. W. Crofton and T. D. Hain, “Environmental considerations for xenon electric propulsion,” in *the 30th International Electric Propulsion Conference, IEPC-2007-257*, 2007.
- [54] R. WELLE, “Availability considerations in the selection of inert propellants for ion engines,” in *21st International Electric Propulsion Conference*, 1990, p. 2589.

- [55] “Linde engineering, air separation plant,” accessed 15 April 2022. [Online]. Available: <https://www.linde-engineering.com/en/process-plants/air-separation-plants/index.html>
- [56] “Solar sail propulsion: Enabling new destinations for science missions,” accessed 15 April 2022. [Online]. Available: <https://science.nasa.gov/technology/technology-highlights/solar-sail-propulsion-enabling-new-destinations-for-science-missions>
- [57] O. de Weck, “A systems approach to mass budget management,” in *11th AIAA/ISSMO Multidisciplinary Analysis and Optimization Conference*, 2006, p. 7055.

